Development/Plasticity/Repair

The Upregulated Expression of Sonic Hedgehog in Motor Neurons after Rat Facial Nerve Axotomy

Chihiro Akazawa,[1] Hayami Tsuzuki,[1] Yasuko Nakamura,[1] Yo Sasaki,[1] Kanae Ohsaki,[2] Shun Nakamura,[2] Yoshihiro Arakawa,[3] and Shinichi Kohsaka[1]

Departments of [1]Neurochemistry and [2]Biochemistry and Cellular Biology, National Institute of Neuroscience, National Center of Neurology and Psychiatry, Kodaira, Tokyo 187-8502, Japan, and [3]Department of Clinical Research Center, Branch Hospital, Faculty of Medicine, University of Tokyo, Bunkyo-ku, Tokyo 113-8655, Japan

Nerve injury leads to the induction of a large number of genes to repair the damage and to restore synaptic transmission. We have attempted to identify molecules whose mRNA expression is altered in response to facial nerve axotomy. Here we report that facial nerve axotomy upregulates Sonic hedgehog (Shh) and its receptor Smoothened (Smo) in facial motor neurons of adult rats, whereas facial nerve axotomy does not upregulate mRNA of Shh or Smo in neonatal rats. We tested whether overexpression of Shh in facial motor neurons of axotomized neonatal rats may promote neuronal survival. Adenovirus-mediated overexpression of Shh, but not that of β-galactosidase, transiently rescues axotomy-induced neuronal cell death for 3–5 d after axotomy. Finally, the pharmacological inhibitor of Shh signaling, cyclopamine, induces motor neuron death in adult rats after axotomy. These results suggest that Shh plays a regulatory role in nerve injury.

Key words: Shh; neuronal death; axotomy; facial nerve; motor neuron; adenovirus

Introduction

The neuronal responses after peripheral nerve injuries have been intensively characterized and are certainly one of the best characterized models of neuronal regeneration. Facial nerve axotomy of rats, with its extensive abilities to regenerate in adults, provides us with a useful model in which to study the molecular mechanisms of nerve regeneration. It is well known that facial nerve axotomy in neonatal rats induces motor neuron death of the facial nucleus, whereas most of the neurons survive in adult rats (Graeber et al., 1998). The lack of regenerative properties of neonatal rat neurons is partly attributable to insufficient trophic supports from their target (Skene, 1989; Sendtner et al., 1992; Schnell et al., 1994; Yan et al., 1995; Fournier and McKerracher, 1997), but the molecular mechanisms of the axotomy-induced neuronal death in neonatal rats remain to be fully elucidated. To investigate the mechanisms that are responsible for promotion of motor neuron survival, we searched molecules whose mRNA expression is altered after nerve injury. We found that Sonic hedgehog (Shh) expression was significantly upregulated in the cell bodies of motor neurons after facial nerve axotomy.

Shh has been intensively characterized in the developmental stages of various organs, including motor neuron differentiation (Richardson et al., 1997; Pfaff and Kintner, 1998; Briscoe et al., 1999; Soula et al., 2001), limb development (Te Welscher et al., 2002), hair follicle formation, and odondogenesis (St-Jacques et al., 1998). In the developing neural tube, the secretion of Shh from the notochord and floor plate organizes the pattern of ventral neurogenesis along the entire length of the CNS. Shh also plays an important role in the phenotypic specification of ventral neurons. For example, Shh induces the differentiation of motor neurons in the spinal cord and dopaminergic neurons in the midbrain (Tanabe et al., 1995; Pfaff and Kintner, 1998; Briscoe et al., 1999). Although the expression of Shh persists in the adult brain beyond this induction period, little is known about its functional role in adults. A goal of this study is to characterize Shh expression in matured motor neurons after nerve injuries. We performed adenoviral gene transfer of chick Shh to overexpress Shh in the axotomized motor neurons of neonatal rats as a gain-of-function approach. Finally, we analyzed the effect of pharmacological inhibition of Shh signaling in the axotomized motor neurons of adult rats as a loss-of-function approach.

Received Sept. 9, 2003; revised July 12, 2004; accepted July 14, 2004.

This work was supported by grants from the Ministry of Health, Labor, and Welfare, Japan (C.A. and S.K.), from the Ministry of Education, Science, Sports, Culture, and Technology, Japan (C.A. and S.K.), and from the Sankyo Life Science Foundation (C.A.). We thank A. P. McMahon, N. Osumi, and M. Nakafuku for sharing experimental materials. We are grateful to T. M. Jessell and I. Kanazawa for discussion. The anti-Shh monoclonal antibody developed by T. M. Jessell was obtained from the Developmental Studies Hybridoma Bank under the auspices of the National Institute of Child Health and Human Development and maintained by the University of Iowa, Department of Biological Sciences (Iowa City, IA).

Correspondence should be addressed to Chihiro Akazawa, Department of Neurochemistry, National Institute of Neuroscience, National Center of Neurology and Psychiatry, Ogawahigashi 4-1-1, Kodaira, Tokyo 187-8502, Japan. E-mail: akazawa@ncnp.go.jp.

DOI:10.1523/JNEUROSCI.1784-04.2004

 0270-6474/04/247923-08$15.00/0

Materials and Methods

Animals. Adult Wistar rats (200–250 gm) were housed in the animal facility of National Institute of Neuroscience, National Center of Neurology and Psychiatry. The first 24 hr after birth is postnatal day 0 (P0). All animal experiments and care protocols were performed under the approval of the ethical committee on laboratory animals of the institute.

Recombinant adenovirus vectors and Shh antagonist application. The construction and characterization of the adenovirus (AdV) carrying the gene for chick Shh or β-galactosidase (lacZ) was described previously (Ohsaki et al., 2002). The AdV was concentrated by cesium chloride density gradient centrifuge. The concentrated AdV was dialyzed with PBS. Cyclopamine (Toronto Research Chemicals, North York, Ontario,

Canada) or tomatidine (Sigma, St. Louis, MO) was dissolved at a concentration of 1.0 or 5.0 μg/ml in 45% (w/v) 2-hydroxypropyl-β-cyclodextrin (HBC) (Sigma) in PBS (Berman et al., 2002; Lai et al., 2003).

Facial nerve transection. Under ether anesthesia, the facial nerve was transected at the stylomastoid foramen (Graeber et al., 1998). In all experiments, the unoperated contralateral sides serve as a control. For the AdV type V vector, cyclopamine or tomatidine application involved a 1.0 mm^3 Gelfoam (Amersham Biosciences Japan, Tokyo, Japan) soaked with a 1.0×10^{10} multiplicity of infection of AdV, 2 μl of cyclopamine (1.0 or 5.0 μg/ml), or 2 μl of tomatidine implanted immediately at the nerve cut site. After the indicated intervals (6, 12, and 24 hr and 3, 5, 7, and 14 d), rats were killed by cervical decapitation under deep anesthesia by ether. The brains were quickly removed without perfusion and frozen at −70°C until use. Whole series of coronal sections (14-μm-thick cryosections) were taken through the full extent of bilateral facial nuclei. The number of survived motor neurons was determined and counted by a blinded observer as described previously (Baumgartner and Shine, 1997). Five independent experiments were performed, and the total number of survived motor neurons was statistically analyzed (Student's *t* test).

Subtraction cDNA library screening. Five series of pooled facial nuclei were subjected to total RNA isolation by the phenol-guanidine isothiocyanate method. Subtractions between axotomized nuclei and contralateral nuclei were performed by using the SMART subtraction kit (BD Biosciences Clontech, Palo Alto, CA). Three hundred clones were randomly sequenced to identify the insert cDNA.

In situ *hybridization and immunohistochemistry.* The coding region of rat Shh cDNA (accession number, NM_017221) was amplified by PCR using paired primers (5′-ATGCTGCTGCTGCTGGCCAGA-3′ and 5′-TCAGCTGGACTTGACTGCCAT-3′). The cDNA fragments for rat Patched1 (Ptc1) (accession number, AF079162) and rat Smoothened (Smo) (accession number, U84402) were amplified by the paired primers: 5′-ATGCTGAATAAAGCCGAAGT-3′ and 5′-CACGAGGCTGACACAGGGGC-3′ for Ptc1; and 5′-CTTCCGGGACTATGTGCTAT-3′ and 5′-AGAAGTCCGAGTCTGCATCC-3′ for Smo. The amplified fragment was subcloned into a pGEM-T easy vector (Promega, Madison, WI) and subsequently sequenced. Antisense and sense riboprobes were synthesized by transcription using either T7- or SP6-RNA polymerase (Roche Diagnostics, Manheim, Germany) in the presence of digoxigenin-UTP (Roche Diagnostics) for 30 min at 37°C according to the manufacturer's protocol. The digoxigenin-labeled RNA probe was column-purified and reconstituted in distilled water. The 16-μm-thick coronal sections containing bilateral facial nuclei were fixed in 4% paraformaldehyde in 0.1 M PBS for 20 min and washed in PBS, and sections were hybridized overnight at 65°C in a mixture (50% formamide, 10 mM PBS, 20 mM Tris HCl, pH 7.4, 5 mM EDTA, 10% dextransulfate, 1× Denhardt's reagent, 0.2% sodium laurylsarcosine, 500 μg/ml tRNA, and 200 μg/ml sonicated sermon sperm DNA) containing labeled probe (0.5 μg/ml in hybridization mixture). After hybridization, sections were washed in 10 mM dithiothreitol in 5× SSC at 55°C. After washing, alkaline phosphatase-conjugated anti-digoxigenin antibody staining was performed following a chromogenic reaction containing nitroblue tetrazolium and 5-bromo-4-chloro-3-indolylphosphate. After capturing the images, sections were counterstained with Nissl, dehydrated in a graded series of ethanol, and coverslipped with DePeX (BDH Chemicals, Poole, UK).

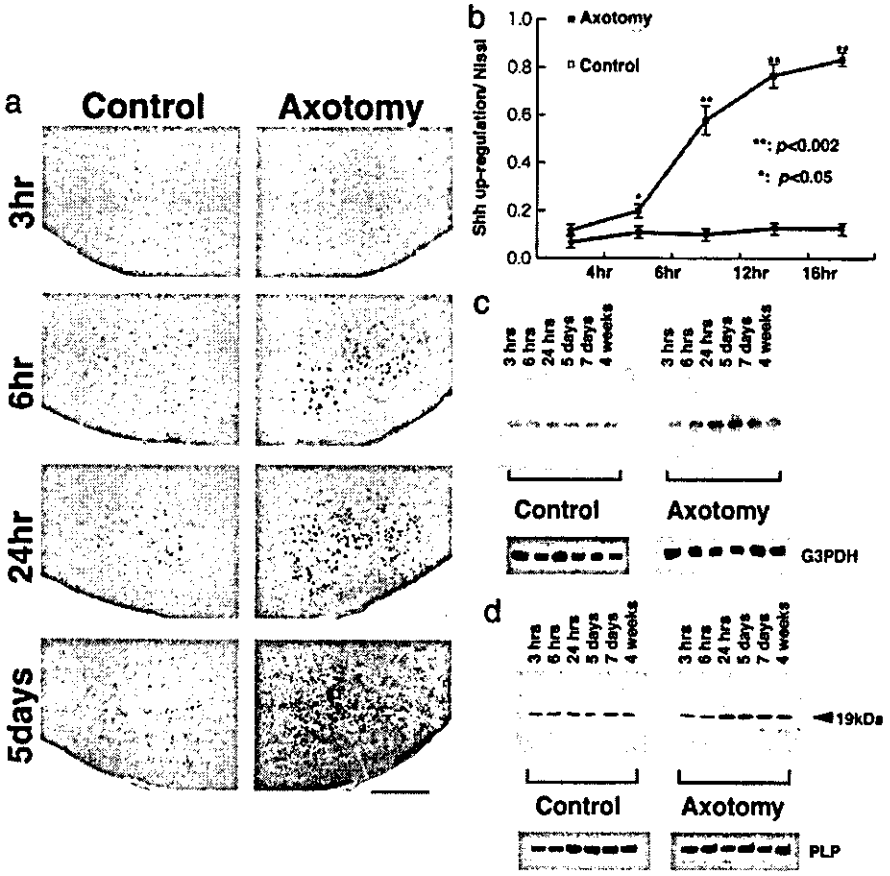

Figure 1. *a*, Upregulated expression of Shh after axotomy in adult rats: *in situ* hybridization of Shh antisense riboprobes in a coronal section at 3, 6, and 24 hr and 5 d after the axotomy. The relatively large size of cells corresponding to motor neurons in facial nucleus shows the expression of Shh mRNAs. Compared with the control side (left), the signal intensity was severalfold higher in the axotomized facial nucleus (right). Scale bar, 500 μm. *b*, After capturing the *in situ* hybridization image, the section was stained with Nissl to calculate the ratio of Shh-upregulated cells. The number of motor neurons that display upregulation of Shh increases to 83 ± 1.4% at 18 hr after the operation. *c*, *d*, Quantitative analyses of Shh expression after axotomy by Northern blot (*c*) and Western blot (*d*) analyses. Each lane contains 30 μg of total RNA (*c*) and 10 μg of total protein (*d*) purified from pooled facial nuclei. Expression of Shh mRNA and 19 kDa polypeptides increased at 24 hr after axotomy and was sustained up to 4 weeks. The control blot using radiolabeled G3PDH for Northern blot and anti-PLP antibody for Western blot revealed that relatively equal amounts of RNA and protein were loaded in each lane.

Double fluorescent-labeling analyses were performed to identify the cellular expression of adenovirus-mediated Shh using mouse monoclonal anti-Shh antibody (5E1; 1:500 dilution; Developmental Studies Hybridoma Bank) in combination with polyclonal antibodies against p75NTR (neurotrophin receptor) (rabbit anti-human p75; 1:1000 dilution; Promega), GAP-43 (growth-associated protein-43) (N-19; goat anti-human GAP-43; 1:2000 dilution; Santa Cruz Biotechnology, Santa Cruz, CA), Iba1 (rabbit anti-Iba1; 1:1000 dilution) (Imai et al., 1996), and GFAP (rabbit anti-GFAP; 1:500 dilution; Dako, Glostrup, Denmark). Cryosections fixed with 4% paraformaldehyde, 0.5% Triton X-100, and PBS were incubated with primary antibodies overnight at 4°C and washed and incubated with the secondary antibodies. Fluorescent images were captured by using a Leica confocal microscope (TSC-SP2; Leica Microsystems, Wetzler, Germany).

Northern and Western blotting. Rat facial motor nuclei (five pooled animals) were homogenized in 100 μl of lysis buffer (50 mM HEPES, pH 7.5, 150 mM NaCl, 1.5 mM $MgCl_2$, 5 mM EGTA, 10% glycerin, 1% Triton X-100, 0.1 mM Na_3VO_4, 10 μg/ml aprotinine, 10 μg/ml leupeptine, and 1 mM phenylmethylsulfonyl fluoride). Lysates were then centrifuged at 12,000 × *g* for 20 min at 4°C. The protein concentration was quantified using a modification of the Bradford assay (Bio-Rad, Munich, Germany). Total cell lysate (10 μg) was electrophoresed through 7.5% SDS

polyacrylamide gels and electroblotted on nitrocellulose membranes (Schleicher & Schnell, Dassel, Germany). The blots were incubated overnight at 4°C with rabbit anti-Shh (1:2000; a generous gift from A. P. McMahon, Harvard University, Cambridge, MA) or anti-goat anti-myelin proteolipid protein (PLP) (Santa Cruz Biotechnology) in 10 mM Tris HCl, pH 8.0, 150 mM NaCl, and 0.05% Tween 20 containing 1% BSA.

RNase protection assay. For detection of Smoothened and Patched mRNA, equal amounts of total RNA (30 μg) were subjected to RNase protection assay as described previously (Funakoshi et al., 1993). Radiolabeled antisense riboprobes were generated in the presence of [γ-^{32}P]CTP using SP6- or T7-RNA polymerase. Glyceraldehyde 3-phosphate dehydrogenase (G3PDH) was used for subsequent standardization. After the RNase digestion, protected fragments were separated in urea-denatured 4% polyacrylamide gels and exposed to x-ray films with intensifying screens at −70°C.

Results

Identification of Shh as an upregulated molecule after facial nerve axotomy

We sequenced 300 clones from the subtraction cDNA library between axotomized and contralateral facial nuclei at 24 hr after axotomy. By searching the BLAST database, 182 clones were identical to transcripts from known genes, and 118 clones were unknown (data not shown). Some of the known genes, such as galectin-1 (Akazawa et al., 2004), GFRα-1 (glial cell line-derived neurotrophic factor family receptor α1) (Tsujino et al., 1999), GLT-1 (glutamate transporter-1) (Lopez-Redondo et al., 2000), p75NTR (Gschwendtner et al., 2003), and GAP-43 (Doster et al., 1991), were already described as upregulated after axotomy of facial or hypoglossal nerves. We found four transcripts of Shh and one transcript of Smo as upregulated molecules.

Upregulation of Shh in the facial motor neurons of adult rats

In situ hybridization was performed to characterize the cellular expression of Shh after facial nerve axotomy. The motor neurons of adult facial nucleus express Shh mRNA at a low level (Fig. 1*a*, Control). On the side of axotomy, facial motor neurons started to show Shh transcripts at 6 hr after the operation. The expression of Shh reached its peak at 24 hr and continued at high levels until 4 weeks after the operation. To quantify the population of Shh-upregulated motor neurons in the axotomized facial nucleus, the sections were counterstained by Nissl to identify motor neurons. The number of neurons that upregulated Shh transcripts and the number of Nissl-positive cells were counted in the same sections, and the ratio was shown (Fig. 1*b*). Almost 83 ± 1.4% of Nissl-positive neurons upregulated Shh at 18 hr after the axotomy, whereas in the control side, <20% of Nissl-positive neurons express Shh. To semiquantify the Shh increase, we performed Northern blot analysis for the total RNA purified from pooled facial nuclei from five independent experiments (Fig. 1*c*). Transcripts of Shh were present at a low level at 3 hr after axotomy. The initial increase was detected at 6 hr and reached its peak at ~24 hr, followed by a subsequent decline. We next tested the protein expression of Shh by Western blot analysis. The 19 kDa single band was detected, and the expression increased from 24 hr after axotomy and was sustained for up to 1 month (Fig. 1*d*). From these experiments, facial nerve axotomy induces the expression of Shh transcripts and proteins in motor neurons of adult rats.

Upregulation of Smo after axotomy

The Shh receptor consists of at least two components, Ptc1 for ligand binding and Smo for downstream signaling (Ho and Scott, 2002). We next tested whether axotomy of adult rats alters the expression of the Shh receptor. We performed RNase protection analysis to detect the transcripts of Smo, Ptc1, and G3PDH, respectively (Fig. 2*a*). Radiolabeled antisense riboprobes corresponding to the 384 bp of Smo, 442 bp of Ptc1, and 410 bp of G3PDH yielded 302, 300, and 302 bp of protected band after RNase digestion, respectively. The expression of Smo mRNA was upregulated at 24 hr after axotomy, whereas no change in Ptc1 and G3PDH expression was observed between axotomized and control facial nuclei. The intensity of protected bands in G3PDH showed that relatively equal amounts of RNA were used in the experiments. To further investigate the cellular expression of Smo, *in situ* hybridization histochemistry was performed (Fig. 2*b*). The Smo mRNA was detected in the facial motor neurons of the control side, albeit at a low level. Facial nerve axotomy of adult rats induced upregulated expression of Smo mRNA in the motor neurons at 24 hr after axotomy. No upregulated expression of Ptc1 mRNA was detected by *in situ* hybridization (data not shown).

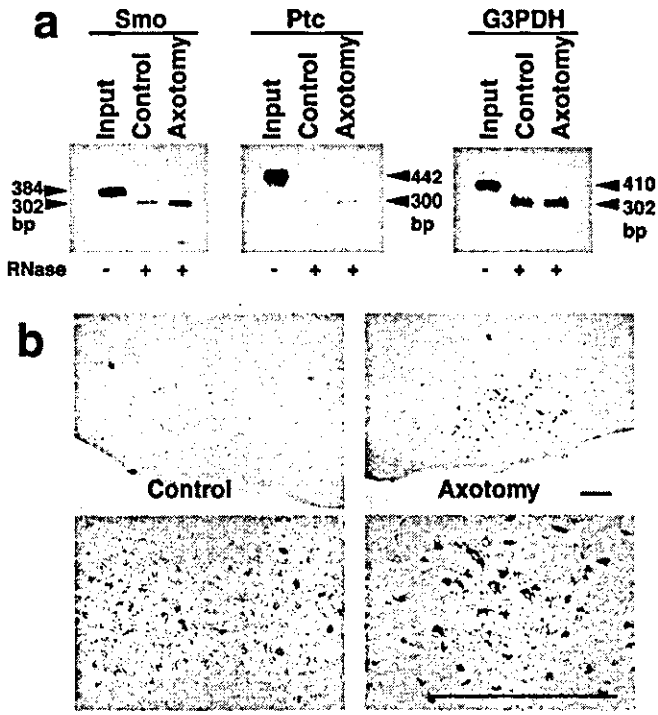

Figure 2. Expression of the Shh receptor Smo and Ptc in the facial nucleus of control and axotomized adult rats at 24 hr after axotomy. *a*, The total RNA (30 μg) purified from pooled facial nuclei was subjected to RNase protection analyses. For the expression of Smo, a 384 bp antisense riboprobe was hybridized, and a 302 bp band was protected after RNase digestion. For the expression of Ptc1, a 442 bp antisense riboprobe yielded a 300 bp protected band after RNase digestion. Control experiments using a G3PDH antisense riboprobe showed that equal amounts of total RNA were used in these experiments. *b*, *In situ* hybridization histochemistry showing the cellular localization of Smo transcripts in facial nucleus. The axotomy of adult rat facial nerve induced upregulated expression of Smo mRNA in the cell bodies of motor neurons. Scale bar, 500 μm.

No upregulation of Shh and Smo in neonatal rats

It is well characterized that neonatal facial nerve axotomy induces motor neuron cell death ~5 d after axotomy. We next tested whether Shh expression was upregulated in neonates after axotomy. Although the basal level of Shh expression was detected in cell bodies of motor neurons at P2, that is, 24 hr after axotomy (Fig. 3*a*, Control), the facial nerve axotomy did not induce Shh expression (Fig. 3*a*, Axotomy). To further investigate the time course and semiquantification of molecules after axotomy, Northern and Western blot analyses were performed by using

total RNA and total protein lysates purified from facial nuclei collected from five independent experiments. No upregulation of Shh transcripts and polypeptides was detected after axotomy of neonatal rats (Fig. 3*b*,*c*). The Shh expression was not detected 5 d after axotomy in the axotomized facial nuclei. This is because of the axotomy-induced neuronal death in neonates. We next tested whether axotomy of neonatal rats alters the expression level of Smo by RNase protection analysis. The protected bands were clearly detected for both Smo and Ptc1, although there was no change of expression between control and axotomized facial nuclei (Fig. 3*d*). Neonatal rats lack the upregulation of both Shh and Smo after axotomy.

Motor neuron survival promoted by Shh–adenovirus in neonatal rats

To test the possibility that the upregulated expression of Shh may relate to the survival of axotomized motor neurons, we implanted a Gelfoam (1.0 mm^3) soaked with a 1×10^{10} multiplicity of infection of AdV vector containing chick Shh (AdV–Shh) (Ohsaki et al., 2002) or β-galactosidase (AdV–lacZ) at the proximal stump of facial nerve immediately after the bilateral axotomy. First, to test the efficacy of gene transfer by AdV, we compared the lacZ staining after the operation of neonatal and adult rats. Operations were performed at P1 and adult (200–250 gm), and Gelfoams soaked with AdV–lacZ were implanted. We found that AdV-mediated gene transfer is more effective in neonatal rats than in adult rats (see Fig. 6*a*). Thus, we used neonatal rats for the exogenous overexpression of Shh. We applied the AdV–Shh to the right side of the axotomized nerve stump and the AdV–lacZ to the left side. Pups were treated for 4 d and then killed for sectioning. The sections were double-stained with anti-Shh rabbit polyclonal antibody and anti-lacZ monoclonal antibody and visualized with Alexa-Fluor 488- and Alexa-Fluor 594-conjugated secondary antibodies, respectively. After capturing the confocal images, the sections were stained with Nissl to obtain neuronal nuclear staining. There is a significant increase of Nissl staining-positive cells in the AdV–Shh-infected side (Fig. 4*b*) compared with the AdV–lacZ-infected side (Fig. 4*a*). Antibody staining showed the overexpressed Shh was only detected in the AdV–Shh-infected side (Fig. 4*d*). When we compared the Nissl staining with anti-Shh staining, Shh-transferred motor neurons formed a cluster-like staining. Western blotting analysis confirmed the overexpression of chick Shh only in the AdV–Shh-infected side (data not shown).

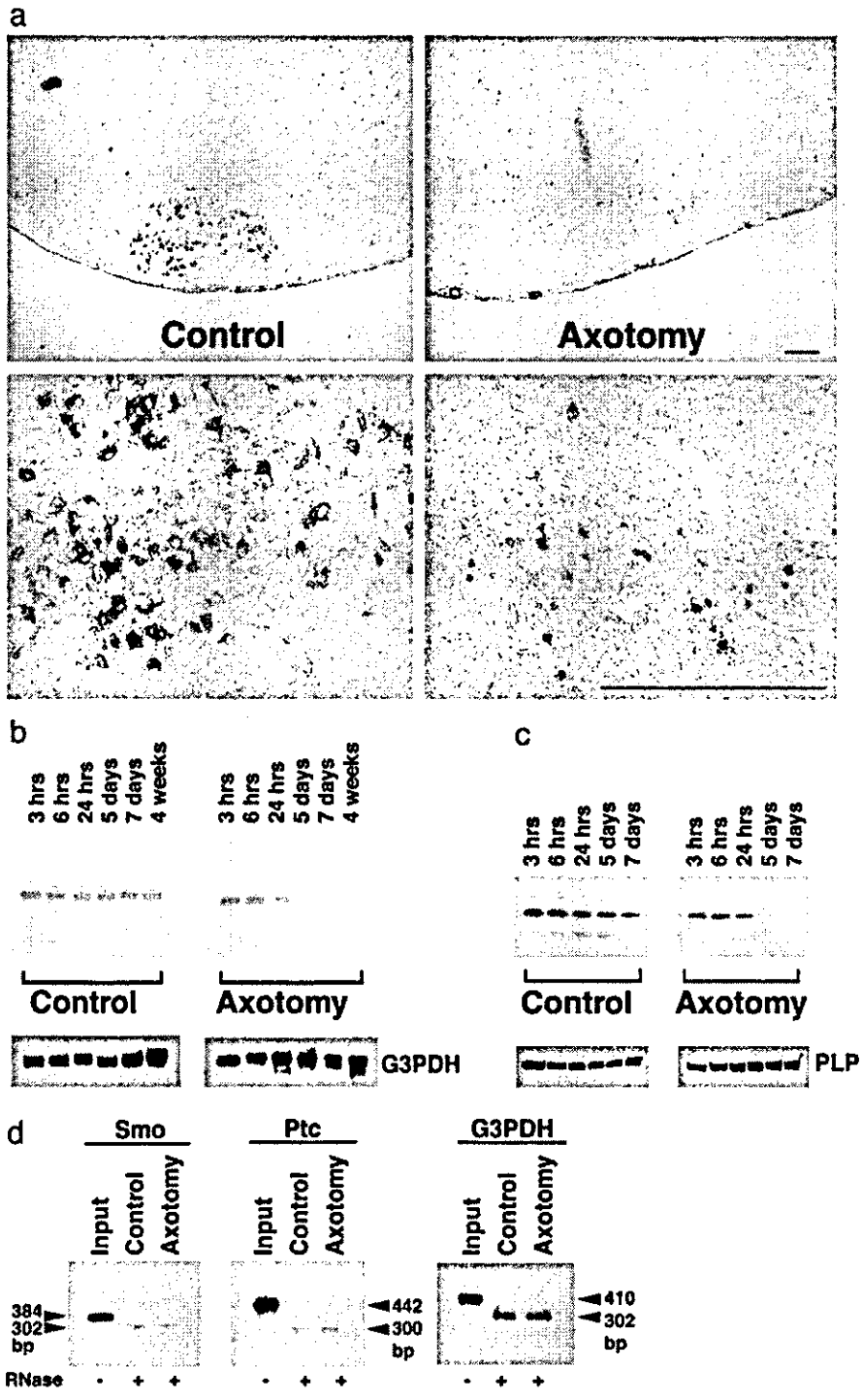

Figure 3. *a*, *In situ* hybridization histochemistry of Shh in neonatal rats at 24 hr after axotomy. The control side of facial motor neurons expresses Shh mRNA at a low level, whereas axotomy of facial nerves rather suppresses the Shh expression. Scale bar, 100 μm. *b*, *c*, Quantitative analyses of Shh expression after axotomy by Northern blot (*b*) and Western blot (*c*) analyses. Each lane contains 30 μg of total RNA (*b*) and 10 μg of total protein lysates (*c*) purified from pooled facial nuclei corresponding to representative time course. No expression of Shh mRNA and protein was detected in the facial nuclei after 5 d in axotomized neonatal rats because the axotomy of neonatal rats induces motor neuron death. Control blots were performed using radiolabeled G3PDH or anti-PLP antibody. *d*, The RNase protection analysis revealed that axotomy of neonatal rat facial nerves did not induce the expression of Smo and Ptc1 mRNA.

To identify the cell types infected with AdV–Shh, fluorescent double staining was performed in neonatal rats. The immunoreactivities of anti-Shh monoclonal antibody were visualized with the secondary antibody conjugated with Alexa-Fluor 488 (Fig. 5, green). Rabbit polyclonal antibodies against p75NTR or GAP-43

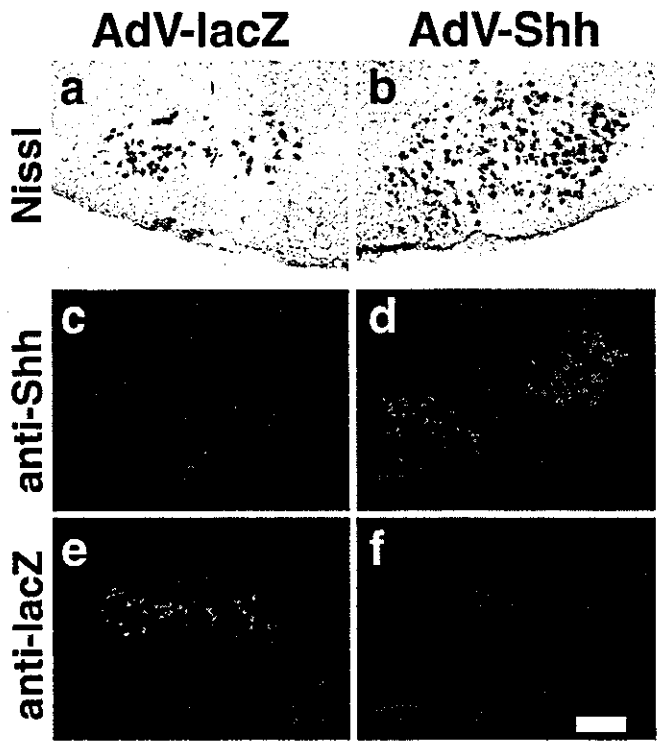

Figure 4. We tested the effect of Shh overexpression in neonatal rats by the implantation of Gelfoams containing AdV–lacZ in the left operation side and Gelfoams containing AdV–Shh in the right operation side. At 3 d after the operation, the cryosections were stained with rabbit polyclonal anti-Shh (*c*, *d*) and mouse monoclonal anti-lacZ (*e*, *f*) antibodies visualized with Alexa-Fluor 488-conjugated (green) and Alexa-Fluor 594-conjugated (red) secondary antibodies. After capturing the confocal images, sections were stained with Nissl to visualize the neuronal nuclear staining (*a*, *b*). Five independent experiments were performed, and a representative result is shown. Scale bar, 500 μm.

were used to identify the motor neurons of facial nucleus. For non-neuronal marker stainings, rabbit polyclonal antibodies against Iba1 or GFAP were used. The immunoreactivities of neuronal or non-neuronal markers were visualized by the secondary antibody conjugated with Alexa-Fluor 594 (Fig. 5, red). The expression of Shh (Fig. 5, arrows), which was only detected in the lesioned facial nuclei, overlapped well with the immunoreactivities of p75NTR or GAP-43. Meanwhile, non-neuronal markers, such as Iba1 that localizes in the cell bodies of microglia–macrophage (Fig. 5, m) and GFAP that localizes in astrocytes (Fig. 5, a), were barely detected in the Shh-positive cells.

Time course of survival-promoting effect of Shh overexpression in neonatal rats

Given the potent *in vitro* action of AdV–Shh on axotomized motor neurons of neonates, we next looked for the time course of this effect (Fig. 6*b*). At 4 d after the operation, lesioned neonates that were treated with AdV–lacZ retained only $0.37 \pm 0.07 \times 10^4$ cells of their facial motor neurons. In contrast, the lesioned facial nuclei that received AdV–Shh showed $0.88 \pm 0.07 \times 10^4$ cells stained with Nissl, undistinguishable from the nonlesioned side. The difference in neuronal survivals between the AdV–Shh and AdV–lacZ was statistically significant ($n = 5$; $t = 21.9$; $p < 0.001$). However, this effect was only retained for 1 week. At 2 weeks after the operation, the motor neurons that received AdV–Shh finally shrank, and the cellular organization of the facial nucleus was no longer observed. Thus, AdV–Shh can prevent death of axotomized neonatal motor neurons, although this is transient and insufficient to attenuate the full survival. To exclude the toxicity of AdV treatment, we compared the number of the Nissl-positive neurons between the AdV–lacZ-infected facial nuclei and PBS-applied facial nuclei. There is no significant difference in the number of survived cells between AdV-infected neurons and PBS-applied neurons (Fig. 6*c*). This means that there is no toxic effect of AdV, and the survival of our current result may be solely attributable to the overexpression of Shh.

Inhibition of Shh signaling in adult rat axotomy

To examine whether the inhibition of Shh signaling would reduce the regeneration of axotomized motor neurons in adult rats, the Gelfoam was soaked with cyclopamine, a specific inhibitor of Shh signaling shown to act by direct binding to the heptahelical bundle of Smo (Chen et al., 2002b), tomatidine (Berman et al., 2002), an inactive analog of cyclopamine, or with the vehicle HBC and implanted at the axotomized region. HBC has been extensively used to increase the solubility of hydrophobic compounds for delivery to the brain with no observed side effects (Lai et al., 2003). At 7 d after the implantation of cyclopamine, tomatidine, or vehicle alone, sections covering bilateral facial nuclei were prepared, and the total number of Nissl-positive motor neurons was counted. Five independent rats were operated on and subjected to the statistical analyses (Student's *t* test). The implanted cyclopamine reduced the number of Nissl-positive neurons by ~60% in a dose-dependent manner compared with the control vehicle side (Fig. 7). Meanwhile, the implanted tomatidine did not influence the number of Nissl-positive neurons.

Discussion

Nerve injuries induce a variety of molecular responses such as neurotrophic factors, cytokines, growth factors, and extracellular molecules that may be involved to some extent in the regeneration of injured neurons (Skene, 1989; Doster et al., 1991; Sendtner et al., 1992; Schnell et al., 1994; Yan et al., 1995; Fournier and McKerracher, 1997). In the course of searching the molecules whose expression is altered in adult rat motor neurons of facial nucleus after axotomy, we found that Shh expression was upregulated from 24 hr after axotomy and declined at 4 weeks. The physiological roles of Shh have been intensively characterized in vertebrate development. It specifies the identity of different cell types in the ventral neural tube in early development (Pfaff and Kintner, 1998; Briscoe et al., 1999; Oppenheim et al., 1999). Although Shh is strong in inducing motor neurons from progenitor cells, there have been few reports characterizing its role in matured neurons (Miao et al., 1997; Traiffort et al., 1998, 1999; Ho and Scott, 2002). This is the first evidence that nerve axotomy induces upregulation of both Shh and Smo. This coordinated expression pattern, of both the ligand and receptor, in adult motor neurons strongly suggests that Shh may act on motor neurons in an autocrine manner. Another possibility is that Shh may act on their surrounding cells such as astrocytes, microglial cells, and Schwann cells to release molecules mediating motor neuron survival. Although the precise molecular circuit still remains unclear, our findings imply the novel function of Shh in matured motor neurons altering its expression level after nerve injury. Recently, new roles of Shh have been intensively characterized. In the adult hippocampus, Shh has been shown as a regulator of stem cell proliferation (Lai et al., 2003). It was also reported that Shh can directly attract spinal cord axons and commissural axons as a chemoattractant (Trousse et al., 2001; Charron et al., 2003). It is interesting that, in addition to its earlier role in development, Shh may function later in a novel role in the adult brain. Addi-

tional studies will confirm how widely this key molecule is used not just in the embryo but also in the adult nervous system.

It has not been fully elucidated why axotomy of neonatal rats results in the cell death of motor neurons, whereas axotomy of adult rats results in successful regeneration (Graeber et al., 1998). Although a number of molecules involved in the repair process have been identified and characterized, the precise timing of these cascades may be critical to understand the process of nerve regeneration. We found a quite contrasting result that only adult rat axotomy induces the upregulation of Shh and Smo expression, whereas neonatal rat axotomy does not. Thus, we tested the gain of function of Shh on axotomized neonatal rats. We observed that AdV-mediated gene transfer of Shh after axotomy of neonatal rats transiently endows the axotomized motor neurons with the ability to survive. The modified AdV used in our studies infects cells through a receptor-mediated mechanism. AdV vectors can infect cells *in vivo* to express a high level of the transgene within hours after infection (Moriyoshi et al., 1996; Verma and Somia, 1997). In somatic tissues, the expression sometimes lasts for 5–10 d after infection, attributable in part to viral-induced immune responses of the recipients. In fact, there are also reports describing a relatively limited period of gene transfer via AdV vectors (Baumgartner and Shine, 1998; Hottinger et al., 2000). In our experiments, it is possible that the survival-promoting effect of Shh is influenced by adenovirus toxicity, limiting the number and the duration of survived neurons. The modification of viral vector and transfer methods is necessary to improve the efficacy of regeneration. Alternatively, the development of pharmacological agonist–antagonist Shh signaling will be also beneficial if oral treatment is effective, as described recently (Chen et al., 2002a; Machold et al., 2003).

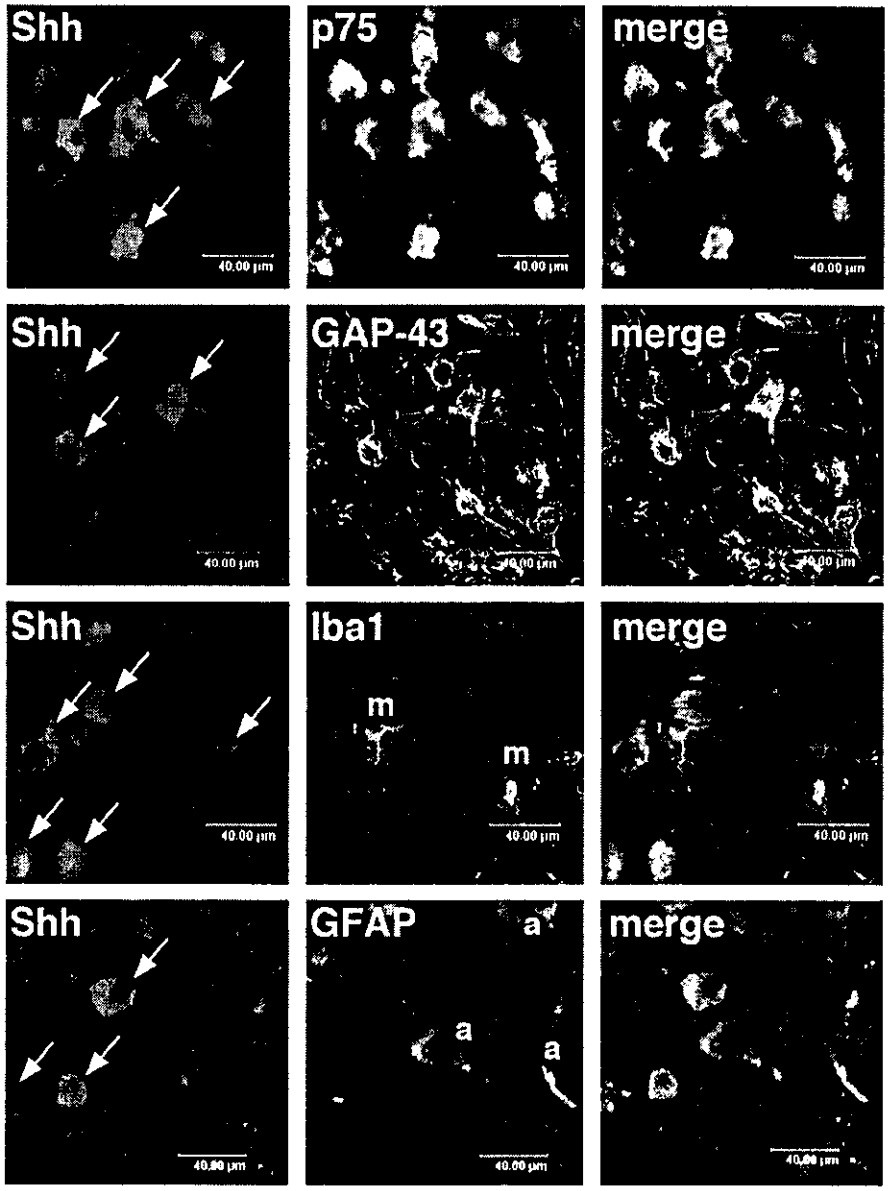

Figure 5. Cellular localization of adenovirus-mediated Shh expression in the lesioned facial nuclei of neonatal rats. The immunoreactivities of the anti-Shh monoclonal antibody were visualized with Alexa-Fluor 488 (green, left). The neuronal (p75 and GAP-43) and non-neuronal (m, Iba1 for microglia and macrophage; a, GFAP for astrocyte) markers were visualized with Alexa-Fluor 594 (red, middle). Shh immunoreactivities (arrows) were observed in the cell bodies of p75-positive or GAP-43-positive neurons but not detected in the cell bodies of Iba1-positive (m) or GFAP-positive (a) cells. Scale bar, 40 μm.

We assessed the cellular expression of AdV–Shh in the lesioned facial nucleus. Immunoreactivities of Shh were strongly observed in the cell bodies of facial motor neurons but were not detected in the cell bodies of astrocytes or microglia. Based on our current observations, the selective upregulation of Shh and Smo in axotomized motor neurons may serve in multiple pathways. The Shh may function as a survival factor per se in an autocrine manner. The motor neurons in response to the Shh may influence surrounding cells through unidentified molecules. Alternatively, the secreted Shh may directly affect surrounding cells, although, at least in our experimental conditions, the expression of Ptc1 and Smo was under the detection level in glial cells. In this paper, we described the immunoreactivities of Iba1 that resides in microglia, and microglia-derived macrophages were detected in the cells adjacent to Shh-positive motor neurons. Phagocytic microglia surround the injured neurons to remove the lethally damaged neurons to preserve functional and structural architects of the lesioned nervous system (Graeber et al., 1998). Additional studies on Shh signaling will clarify how precisely the cellular network is preserved in nerve regeneration.

Although exogenous Shh promotes the transient survival of axotomized motor neurons of neonatal rats, this does not answer the question of whether the endogenous Shh is involved in the regeneration of axotomized neurons. We used the steroidal alkaloid cyclopamine, which is known to inhibit the Shh signaling through the specific binding of cyclopamine and Smo, altering the signal transduction of Smo (Chen et al., 2002b). In the axotomized adult rats, the application of cyclopamine adjacent to the nerve cut site significantly reduced the number of Nissl-positive motor neurons in a dose-dependent manner, whereas its inactive analog tomatidine had no effect. Taken together with our present

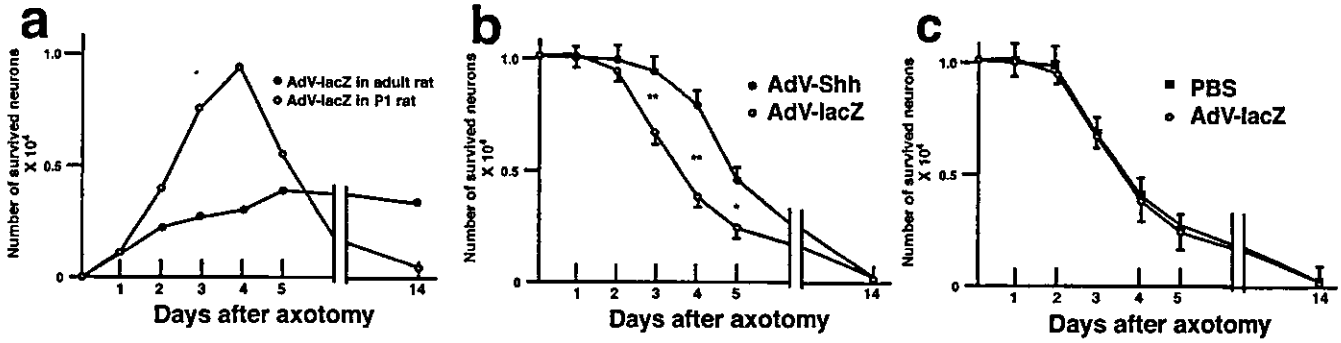

Figure 6. *a*, Efficacy of adenovirus-mediated overexpression of lacZ after axotomy in P1 and adult rats in the lesioned motor neurons. The pups were treated for 4 d after axotomy after the implantation of gelfoams containing AdV–lacZ. The number of lacZ-positive neurons was counted. In the neonatal rats, more lacZ-positive neurons were observed than in the adult rats by the adenovirus gene transfer. The number of Nissl-positive survived neurons was counted from the sections covering bilateral facial nuclei. Results of three independent experiments were subjected to statistical analysis (Student's *t* test, $*p < 0.01$; $**p < 0.001$). Shh–adenovirus significantly potentiates the survival of axotomized motor neurons from 3 to 5 d after axotomy and adenovirus application (*a*). An application of adenovirus after axotomy did not influence the number of survived neurons compared with PBS application (*b*).

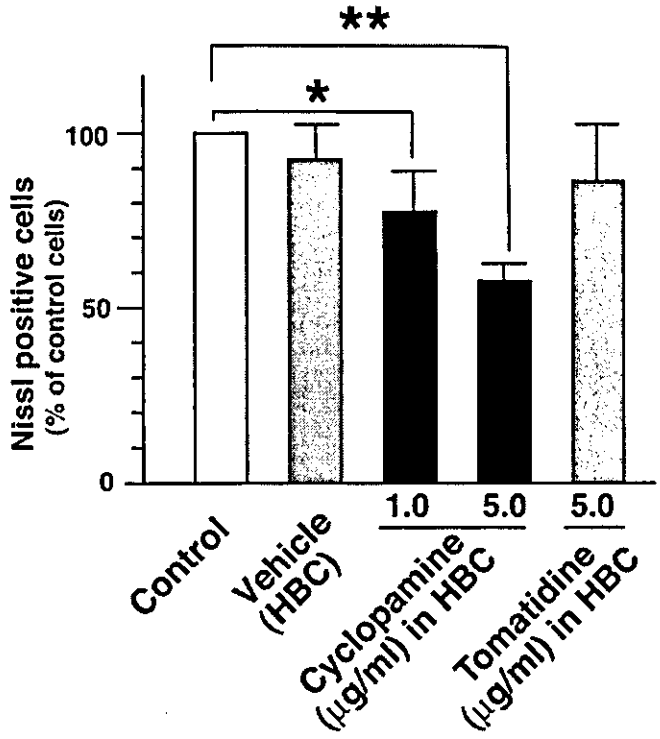

Figure 7. Inhibition of Shh signaling in axotomized adult rats. The cyclopamine application resulted in the loss of motor neurons *in vivo*. Bilateral facial nerves were axotomized and a Gelfoam soaked with cyclopamine (1.0 or 5.0 μg/ml), with tomatidine (5.0 μg/ml), or with vehicle (45% w/v HBC) was implanted in each side. The total number of Nissl-positive cells was counted and compared between the implanted side and the control side. Five independent animals were operated on and statistically analyzed by Student's *t* test ($*p < 0.05$; $**p < 0.01$).

result, it is strongly suggested that endogenous Shh plays an important role in the adult brain, and this represents one of the few demonstrations of Shh function in the adult brain.

Our findings suggest that in addition to its earlier role in directing cellular fates in development, Shh functions as a regulatory role after nerve injury. This adds to a rapidly growing list of factors that have been identified as key molecules in nerve regeneration. Although considerable progress has been made in recent years in defining the genetic and molecular control of nerve regeneration, characterization in detail of molecular cascades has lagged. Our results *in vivo* have a therapeutic implication of Shh for regeneration of neuronal tissues after injuries. Based on our *in vivo* studies, besides its well characterized effects during development, we propose the *de novo* function of Shh in the regeneration of injured motor neurons.

References

Akazawa C, Nakamura Y, Sango K, Horie H, Kohsaka S (2004) Distribution of the galectin-1 mRNA in the rat nervous system: its transient upregulation in rat facial motor neurons after facial nerve axotomy. Neuroscience 125:171–178.

Baumgartner BJ, Shine HD (1997) Targeted transduction of CNS neurons with adenoviral vectors carrying neurotrophic factor genes confers neuroprotection that exceeds the transduced population. J Neurosci 17:6504–6511.

Baumgartner BJ, Shine HD (1998) Permanent rescue of lesioned neonatal motoneurons and enhanced axonal regeneration by adenovirus-mediated expression of glial cell-line-derived neurotrophic factor. J Neurosci Res 54:766–777.

Berman DM, Karhadkar SS, Hallahan AR, Pritchard JI, Eberhart CG, Watkins DN, Chen JK, Cooper MK, Taipale J, Olson JM, Beachy PA (2002) Medulloblastoma growth inhibition by hedgehog pathway blockade. Science 297:1559–1561.

Briscoe J, Sussel L, Serup P, Hartigan-O'Connor D, Jessell TM, Rubenstein JL, Ericson J (1999) Homeobox gene Nkx2.2 and specification of neuronal identity by graded Sonic hedgehog signaling. Nature 398:622–627.

Charron F, Stein E, Jeong J, McMahon AP, Tessier-Lavigne M (2003) The morphogen Sonic hedgehog is an axonal chemoattractant that collaborates with netrin-1 in midline axon guidance. Cell 113:11–23.

Chen JK, Taipale J, Young KE, Maiti T, Beachy PA (2002a) Small molecule modulation of Smoothened activity. Proc Natl Acad Sci USA 99:14071–14076.

Chen JK, Taipale J, Cooper MK, Beachy PA (2002b) Inhibition of Hedgehog signaling by direct binding of cyclopamine to Smoothened. Genes Dev 16:2743–2748.

Doster SK, Lozano AM, Aguayo AJ, Willard MB (1991) Expression of the growth-associated protein GAP-43 in adult rat retinal ganglion cells following axon injury. Neuron 6:635–647.

Fournier AE, McKerracher L (1997) Expression of specific tubulin isotypes increases during regeneration of injured CNS neurons, but not after the application of brain-derived neurotrophic factor (BDNF). J Neurosci 17:4623–4632.

Funakoshi H, Frisen J, Barbany G, Timmusk T, Zachrisson O, Verge VM, Persson H (1993) Differential expression of mRNAs for neurotrophins and their receptors after axotomy of the sciatic nerve. J Cell Biol 123:455–465.

Graeber MB, Lopez-Redondo F, Ikoma E, Ishikawa M, Imai Y, Nakajima K, Kreutzberg GW, Kohsaka S (1998) The microglia/macrophage response in the neonatal rat facial nucleus following axotomy. Brain Res 813:241–253.

Gschwendtner A, Liu Z, Hucho T, Bohatschek M, Kalla R, Dechant G, Raivich G (2003) Regulation, cellular localization, and function of the p75 neu-

rotrophin receptor (p75NTR) during the regeneration of facial motoneurons. Mol Cell Neurosci 24:307–322.

Ho KS, Scott MP (2002) Sonic hedgehog in the nervous system: functions, modifications and mechanisms. Curr Opin Neurobiol 12:57–63.

Hottinger AF, Azzouz M, Deglon N, Aebischer P, Zurn AD (2000) Complete and long-term rescue of lesioned adult motoneurons by lentiviral-mediated expression of glial cell line-derived neurotrophic factor in the facial nucleus. J Neurosci 20:5587–5593.

Imai Y, Ibata I, Ito D, Ohsawa K, Kohsaka S (1996) A novel gene iba1 in the major histocompatibility complex class III region encoding an EF hand protein expressed in a monocytic lineage. Biochem Biophys Res Commun 224:855–862.

Lai K, Kaspar BK, Gage FH, Schaffer DV (2003) Sonic hedgehog regulates adult neural progenitor proliferation in vitro and in vivo. Nat Neurosci 6:21–27.

Lopez-Redondo F, Nakajima K, Honda S, Kohsaka S (2000) Glutamate transporter GLT-1 is highly expressed in activated microglia following facial nerve axotomy. Brain Res Mol Brain Res 76:429–435.

Machold R, Hayashi S, Rutlin M, Muzumdar MD, Nery S, Corbin JG, Gritli-Linde A, Dellovade T, Porter JA, Rubin LL, Dudek H, McMahon AP, Fishell G (2003) Sonic hedgehog is required for progenitor cell maintenance in telencephalic stem cell niches. Neuron 39:937–950.

Miao N, Wang M, Ott JA, D'Alessandro JS, Woolf TM, Bumcrot DA, Mahanthappa NK, Pang K (1997) Sonic hedgehog promotes the survival of specific CNS neuron populations and protects these cells from toxic insult *in vitro*. J Neurosci 17:5891–5899.

Moriyoshi K, Richards LJ, Akazawa C, O'Leary DD, Nakanishi S (1996) Labeling neural cells using adenoviral gene transfer of membrane-targeted GFP. Neuron 16:255–260.

Ohsaki K, Osumi N, Nakamura S (2002) Altered whisker patterns induced by ectopic expression of Shh are topographically represented by barrels. Brain Res Dev Brain Res 137:159–170.

Oppenheim RW, Homma S, Marti E, Prevette D, Wang S, Yaginuma H, McMahon AP (1999) Modulation of early but not later stages of programmed cell death in embryonic avian spinal cord by sonic hedgehog. Mol Cell Neurosci 13:348–361.

Pfaff S, Kintner C (1998) Neuronal diversification: development of motor neuron subtypes. Curr Opin Neurobiol 8:27–36.

Richardson WD, Pringle NP, Yu WP, Hall AC (1997) Origins of spinal cord oligodendrocytes: possible developmental and evolutionary relationships with motor neurons. Dev Neurosci 19:58–68.

Schnell L, Schneider R, Kolbeck R, Barde YA, Schwab ME (1994) Neurotrophin-3 enhances sprouting of corticospinal tract during development and after adult spinal cord lesion. Nature 367:170–173.

Sendtner M, Holtmann B, Kolbeck R, Thoenen H, Barde YA (1992) Brain-derived neurotrophic factor prevents the death of motoneurons in newborn rats after nerve section. Nature 360:757–759.

Skene JH (1989) Axonal growth-associated proteins. Annu Rev Neurosci 12:127–156.

Soula C, Danesin C, Kan P, Grob M, Poncet C, Cochard P (2001) Distinct sites of origin of oligodendrocytes and somatic motoneurons in the chick spinal cord: oligodendrocytes arise from Nkx2.2-expressing progenitors by a Shh-dependent mechanism. Development 128:1369–1379.

St-Jacques B, Dassule HR, Karavanova I, Botchkarev VA, Li J, Danielian PS, McMahon JA, Lewis PM, Paus R, McMahon AP (1998) Sonic hedgehog signaling is essential for hair development. Curr Biol 8:1058–1068.

Tanabe Y, Roelink H, Jessell TM (1995) Induction of motor neurons by Sonic hedgehog is independent of floor plate differentiation. Curr Biol 5:651–658.

Te Welscher P, Zuniga A, Kuijper S, Drenth T, Goedemans HJ, Meijlink F, Zeller R (2002) Progression of vertebrate limb development through SHH-mediated counteraction of GLI3. Science 298:827–830.

Traiffort E, Charytoniuk DA, Faure H, Ruat M (1998) Regional distribution of Sonic Hedgehog, patched, and smoothened mRNA in the adult rat brain. J Neurochem 70:1327–1330.

Traiffort E, Charytoniuk D, Watroba L, Faure H, Sales N, Ruat M (1999) Discrete localizations of hedgehog signaling components in the developing and adult rat nervous system. Eur J Neurosci 11:3199–3214.

Trousse F, Marti E, Gruss P, Torres M, Bovolenta P (2001) Control of retinal ganglion cell axon growth: a new role for Sonic hedgehog. Development 128:3927–3936.

Tsujino H, Mansur K, Kiryo-Seo S, Namikawa K, Kitahara T, Tanabe K, Ochi T, Kiyama H (1999) Discordant expression of c-Ret and glial cell line-derived neurotrophic factor receptor alpha-1 mRNAs in response to motor nerve injury in neonate rats. Brain Res Mol Brain Res 70:298–303.

Verma IM, Somia N (1997) Gene therapy—promises, problems and prospects. Nature 389:239–242.

Yan Q, Matheson C, Lopez OT (1995) In vivo neurotrophic effects of GDNF on neonatal and adult facial motor neurons. Nature 373:341–344.

Neuroscience 125 (2004) 171–178

DISTRIBUTION OF THE GALECTIN-1 mRNA IN THE RAT NERVOUS SYSTEM: ITS TRANSIENT UPREGULATION IN RAT FACIAL MOTOR NEURONS AFTER FACIAL NERVE AXOTOMY

C. AKAZAWA,[a*] Y. NAKAMURA,[a] K. SANGO,[b] H. HORIE[c] AND S. KOHSAKA[a]

[a]*Department of Neurochemistry, National Institute of Neuroscience, NCNP, Japan, Ogawahigashi 4-1-1, Kodaira, Tokyo 187-8502, Japan*

[b]*Department of Developmental Morphology, Tokyo Metropolitan Institute for Neuroscience, Musashidai 2-6, Fuchu, Tokyo 183-8526, Japan*

[c]*Institute for Biomedical Science, Waseda University, Higashifushimi 2-7-5, Nishi-Tokyo, Tokyo 202-0021, Japan*

Abstract—Galectin-1 is a member of the animal lectin family that displays conserved consensus sequences and similar carbohydrate binding specificities. Recent analyses revealed that galectin-1 plays an important role in the process of nerve regeneration. We analyzed the topological expression of galectin-1 mRNA in adult rat nervous system. Galectin-1 mRNA was predominantly observed in the cell bodies of neurons such as oculomotor nucleus (III), trochlear nucleus (IV), trigeminal motor nucleus (V), abducens nucleus (VI), facial nucleus (VII), hypoglossal nucleus (XII), red nucleus, and locus ceruleus. Neurons in pineal gland and dorsal root ganglia expressed galectin-1 mRNA. We next tested whether the axotomy of facial nerve altered the expression of galectin-1 mRNA in motor neurons. In the adult rats, the axotomy of facial nerve induced transient upregulation of galectin-1 mRNA around 6 h after axotomy. These results indicate that galectin-1 may play roles in the early event of the nerve injury and regeneration through the transient change of its expression level.

Key words: galectin-1, *in situ* hybridization, facial nerve axotomy, motor neuron.

Animal lectins can be classified into two protein families on the basis of their carbohydrate recognition properties (Drickamer, 1988). The first group of calcium-dependent lectins constitutes a large class of integral membrane proteins which include the mammalian asialoglycoprotein receptors and the selectins (Lasky, 1992). The second group of lectins displays the specificity for lactose derivatives in a calcium independent manner (Barondes, 1984). The biological properties of surface carbohydrates have been shown to regulate inflammation, cell adhesion, cell proliferation, cell death, and regeneration of damaged tissues (for review, cf. Hirabayashi and Kasai, 1993; Caron et al., 1990). Galectin, a member of animal lectins, form a molecular family bearing their properties specific for galactosides. Galectins had been called by different names depending on the researchers (e.g. electrolectin, soluble lectins, galaptins, S-Lac lectins, β-galactoside-binding lectins, S-type lectins, etc.), although they have homologous sequences to each other. In order to avoid further inconvenience and confusion, the researchers agreed to use the term galectin (Barondes, 1994). Evidence suggests that the biological activities of the galectins are related to their multivalent binding capacities since most galectins possess two carbohydrate recognition domains. For example, galectin-1 which forms a homomeric dimer binds and cross-links its specific glycoprotein counter-receptors on the surface of human T-cells leading to apoptosis (Amano et al., 2003).

There are several lines of evidence relating galectin-1 to the axonal growth during the developing brain and the nerve regeneration. It was previously reported that galectin-1 localized in the CNS and peripheral nervous system (PNS) in the developmental stages, meanwhile its expression was down-regulated and restricted to PNS in the adult brain (Dodd and Jessell,1986; Hynes et al., 1990). In the olfactory system, galectin-1 has been shown to promote neurite outgrowth in the developing mouse (Puche and Key, 1995). More direct evidence for galectin-1 being involved in axonal growth came from the recent study by using recombinant human galectin-1 to promote axonal regeneration after nerve injury both *in vitro* and *in vivo* (Horie et al., 1999). The non-reducing condition of galectin-1 shows its high potency to promote the axonal regeneration of adult dorsal root ganglia explants at low concentrations (50 pg/ml) that are two orders of magnitude lower than those of the lectin activity of reduced galectin-1, suggesting that galectin-1 may act as a cytokine and not as a lectin.

In the course of analyzing galectin-1 expression, we found that the galectin-1 mRNA was expressed in the discrete population of neurons in adult CNS. Its expression was transiently upregulated in the facial motor neurons after the facial nerve axotomy, suggesting its role after the nerve injury.

*Corresponding author. Tel: +81-423-41-2711; fax: +81-425-67-0518.
E-mail address: akazawa@ncnp.go.jp (C. Akazawa).

Abbreviations: ac, anterior commissure; CA1–3, fields CA1–3 of Ammon's horn; Cb, cerebellar cortex; cc, corpus callosum; CN, deep cerebellar nuclei; Cx, cerebral cortex; DG, dentate gyrus; DR, dorsal raphe nucleus; 4th, 4th ventriculus; Hi, hippocampus; IC, inferior colliculus; MoV, motor trigeminal nucleus; NG, nodose ganglia; OB, main olfactory bulb; Or, stratum oriens; PNS, peripheral nervous system; Po, posterior thalamic nucleus; PR, pontine reticular nucleus; Py, stratum pyramidale; R, red nucleus; Ra, stratum radiatum; SC, superior colliculus; SN, substantia nigra; SSC, sodium chloride/sodium citrate; St, striatum; TG, trigeminal ganglia; Th, thalamus; TM, tuberomammillary nucleus; V, lateral ventricle.

0306-4522/04$30.00+0.00
doi:10.1016/j.neuroscience.2004.01.034

EXPERIMENTAL PROCEDURES

All procedures in this study were approved by the ethical committee upon animal experiments of the National Institute of Neuroscience, NCNP, Japan. The number of animals used was minimized to include only that number needed to ensure reproducibility of results; the suffering was minimized by use of inhaled ether.

Northern blot analysis

Northern blot analyses using ^{32}P-labeled DNA probes was carried out as described previously (Akazawa et al., 1994). The template used for the random primer labeling was the same as used for the riboprobe synthesis for *in situ* hybridization. Total RNA was isolated from pooled materials dissected from the brains of adult Wistar rat by GTC-phenol extraction method as described in detail elsewhere (Chomczynski and Sacchi, 1987), and 30 μg of the total RNA was electrophoresed in a formaldehyde/1.2% agarose gel and transferred to a nylon membrane (Hybond N$^+$; Amersham Biosciences, Piscataway, NJ, USA). The hybridization was carried out at 42 °C containing 50% formamide, 5× sodium chloride/sodium citrate (SSC). The filter was washed under the high stringency of 0.1× SSC, 1% SDS, at 65 °C for 1 h.

In situ hybridization

In situ hybridization was carried out in a way similar to that described elsewhere (Akazawa et al., 1994). Female Wistar rats (200–300 g) were deeply anesthetized with ether and decapitated. Tissues were immediately removed and flash frozen in isopentane at −70 °C. Sections of 14-μm thickness were cut on a cryostat and thaw-mounted onto siran-coated slides, following briefly air-dried and kept in −80 °C until use. Adjacent series of the sections were stained with Nissl and used to confirm the cryoarchitecture and to identify the region in comparison with the references (Paxinos and Watson, 1986).

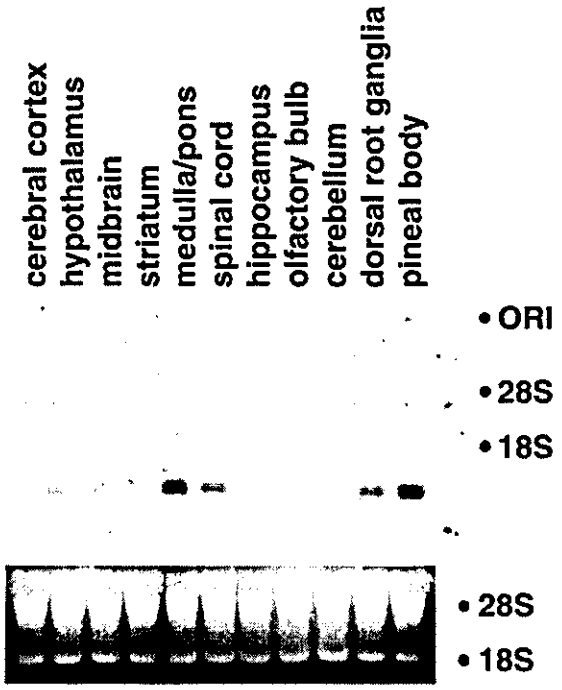

Fig. 1. Northern blot analysis of galectin-1 in rat brain (Top). Each lane contained 30 μg of total RNA purified from the pooled material respectively indicated above. As a molecular size standard, the position of origin (ORI), 28S (5.1 kbp), and 18S (2.0 kbp) were indicated. Ethidium bromide staining of the gel showed that relatively equal amount of RNA with no degradation was loaded in this experiment (bottom).

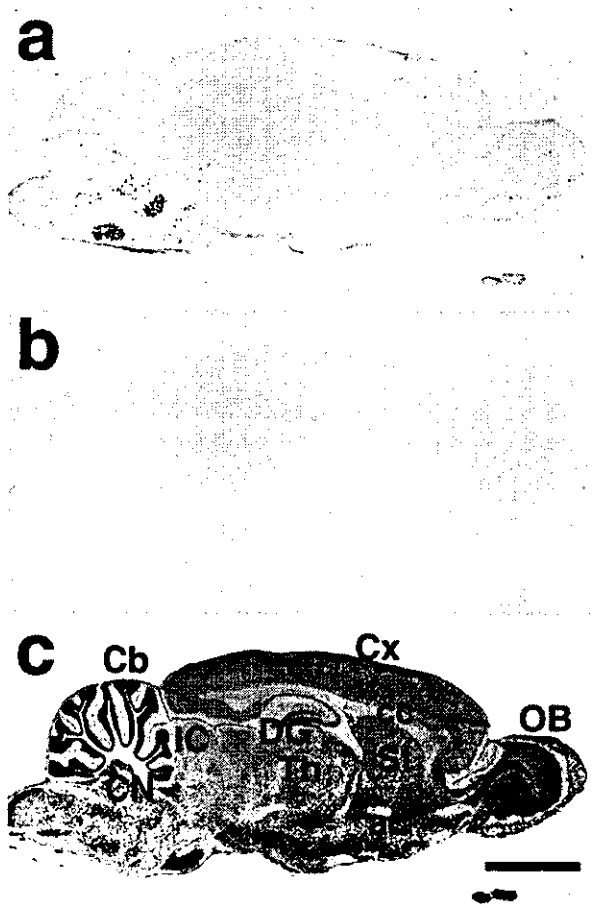

Fig. 2. Distribution of galectin-1 transcripts in the lower magnitude images of parasagittal section of adult rat brain. Sections were hybridized with an antisense riboprobe corresponding to the 408 bp of full-length galectin-1 cDNA (a) or with a sense riboprobe (b). An adjacent section was stained with Nissl (c). Cb, cerebellar cortex; CN, deep cerebellar nuclei; Hi, hippocampus; LS, lateral septal nuclei; OB, main olfactory bulb; RS, retrosplenial cortex; SN, substantia nigra; Th, thalamus. Scale bar=4 mm.

The full coding length of rat Galectin-1 cDNA (408 bp) was amplified by PCR using paired primers (5′-ATGGCCTGTGGTCTGGTCGCC-3′, and 5′-TCACTCAAAGGCCACACACTT-3′). The amplified fragment was subcloned to pGEM-T easy vector (Promega, Madison, WI USA) and subsequently sequenced. The anti-sense and sense riboprobes were synthesized by transcription using either T7 or SP6 RNA-polymerase (Roche Diagnostics GmbH, Mannheim, Germany) in the presence of digoxigenin-UTP (Roche Diagnostics GmbH) for 30 min at 37 °C, according to the manufacturer's protocol. The digoxigenin-labeled RNA probe was column-purified and reconstituted in distilled water at the concentration of 0.1 μg/ml. Sections were fixed in 4% paraformaldehyde in 0.1 M PBS for 20 min, washed in PBS, and hybridized overnight at 65 °C in a mixture (50% formamide, 10 mM PBS, 20 mM Tris–HCl, pH 7.4, 5 mM EDTA, 10% dextran sulfate, 1× Denhardt's reagents, 0.2% sodium lauryl sarcosine, 500 μg/ml t-RNA, 200 μg/ml sonicated single strand-DNA) containing digoxigenin-labeled probe (0.5 μg/μl hybridization mixture). After hybridization, sections were washed in 10 mM dithiothreitol in 5× SCC at 55 °C. After washing, alkaline phosphatase-conjugated anti-digoxigenin antibody staining was performed following the

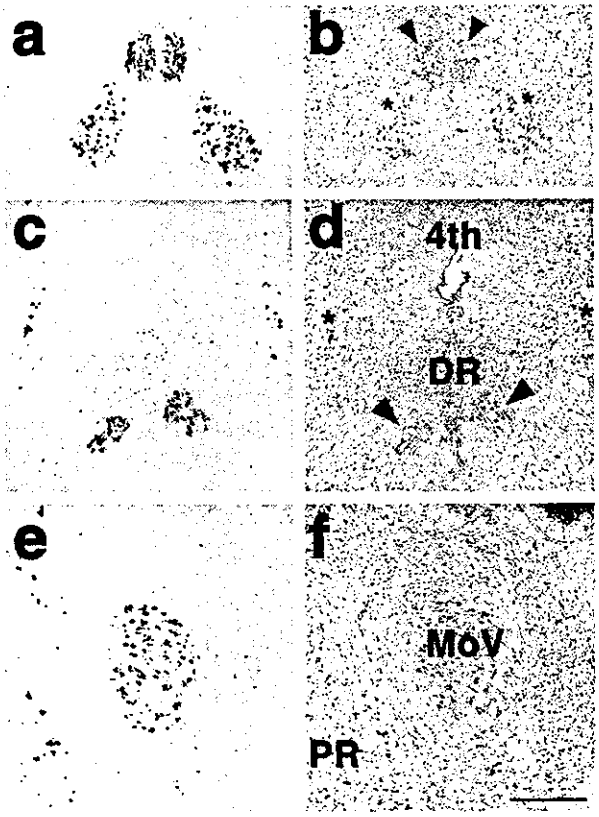

Fig. 3. Hybridization with antisense riboprobe (a, c, and e) and control Nissl staining (b, d, and f) of adult rat coronal sections. Arrowheads in b indicate oculomotor nucleus. * in b indicate red nucleus magnocellulare (a, b). Arrowheads in d indicate trochlear nucleus. * in d indicates mesencephalic trigeminal nucleus. DR, dorsal raphe nucleus; MoV, motor trigeminal nucleus; PR, pontine reticular nucleus; 4th, 4th ventriculus (c, d). Scale bar=0.2 mm.

chromogenic reaction containing Nitroblue Tetrazolium and 5-bromo-4-chloro-3-indolylphosphate. After capturing the images, sections were counter-stained with Nissl, dehydrated in a graded series of ethanol, and coverslipped with DePeX (Gurr; BDH, Poole, UK).

Facial nerve transection

Under ether anesthesia, the facial nerve was transected at the stylomastoid foramen. In all experiments, the un-operated contralateral side served as a control. After the indicated time intervals (3, 6, 9, 12, 24 h), rats were killed under the deep anesthesia by ether. The brains were quickly removed without perfusion and frozen at −70 °C until use. For the Northern blot analysis, bilateral facial nuclei were identified under the microscope, and punched out by 18 gauge needle. Three independent rats were operated and pooled facial nuclei were subjected to the total RNA preparation. Northern blot analysis using 10 μg of total RNA was carried out. The radioactive intensity was measured by BAS5000 image analyzer (Fuji, Tokyo, Japan).

RESULTS

Northern blot analysis

The full coding region of rat galectin-1 was radiolabeled by the random primer labeling method and hybridized with the membrane blotted with 30 μg of total RNA purified from the

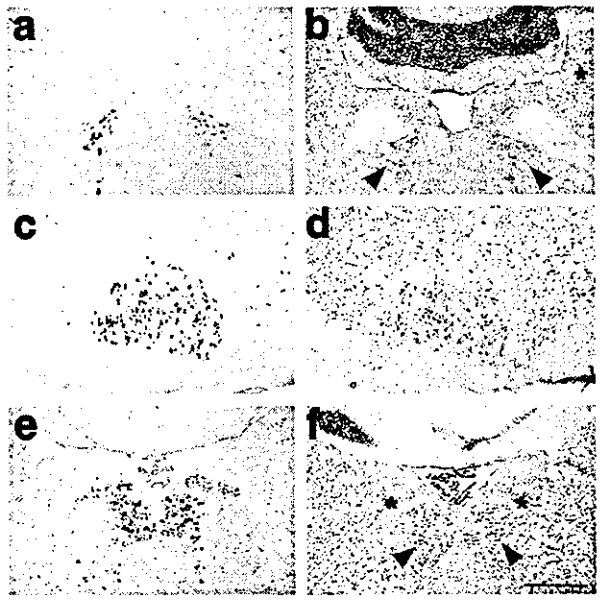

Fig. 4. Hybridization with antisense riboprobe (a, c, and e) and control Nissl staining (b, d, and f) of adult rat coronal sections. Arrowheads in b indicate abducens nucleus. * in b indicates medial vestibular nucleus. Facial nucleus was positively stained with galectin-1 (c, d). Arrowheads in f indicate hypoglossal nucleus. * in f indicates dorsal motor nucleus of vagus. The choroidal plexus was moderately stained with galectin-1 (e, f). Scale bar=0.2 mm.

various brain regions of adult rat. Galectin-1 mRNA was detected as a single band corresponding to the molecular weight of 1,000 base-pairs in the discrete brain regions, such as medulla/pons, pineal body, spinal cord and dorsal root ganglia (Fig. 1, top). Ethidium bromide staining of the gel showed that relatively equal amount of RNA was loaded (Fig. 1, bottom). The band intensity of cerebral cortex and hippocampus was significantly lower than other lanes tested.

In situ hybridization

The digoxigenin-labeled cRNA probe was hybridized with the para-sagittal section of the adult rat. The antisense riboprobes displayed the punctuated staining in the brain stem lesions (Fig. 2a), while no specific staining was detected in the section hybridized with sense ribo-probes hybridized with the adjacent section (Fig. 2b). The hybridization experiment with the same labeled antisense riboprobe in the presence of 100-fold excess of unlabeled probes resulted in no significant signals (data not shown). Neurons expressing galectin-1 mRNA were observed in strictly limited areas throughout the rat brain (summarized in Table 1). The most densely stained cells were seen in the neurons resided at the brainstem. No apparent hybridization signals were observed on glial cells from our experimental condition.

Olfactory system

In the adult rat olfactory bulb, galectin-1 mRNA was detected in mitral cells, external tufted cells, granule cells and cells in the glomerular layer (data not shown), although the

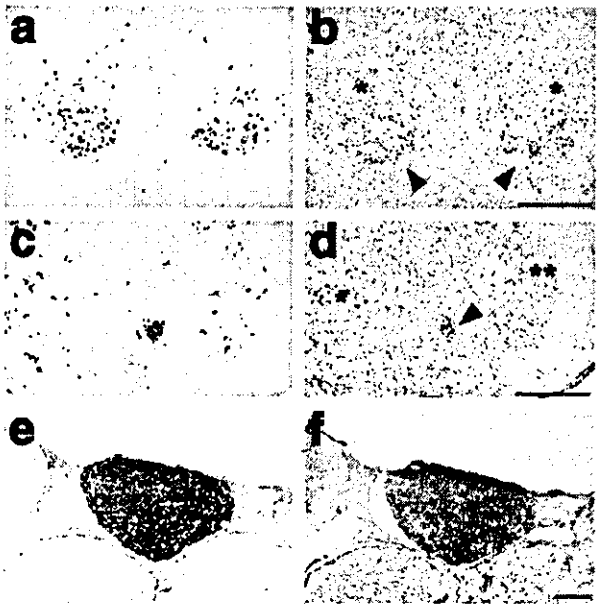

Fig. 5. Hybridization with antisense riboprobe (a, c, and e) and control Nissl staining (b, d, and f) of adult rat coronal sections. Red nucleus complex was positively stained with galectin-1. Arrowheads in b indicate magnocellulare of red nucleus and * in b indicates parvicellular of red nucleus. The arrowhead in d indicates ambiguis nucleus. * intermediate reticular nucleus. ** parvicellular reticular nucleus. Pineal body (epiphysis) was intensely stained with galectin-1 (e, f). Pea mater was moderately stained.

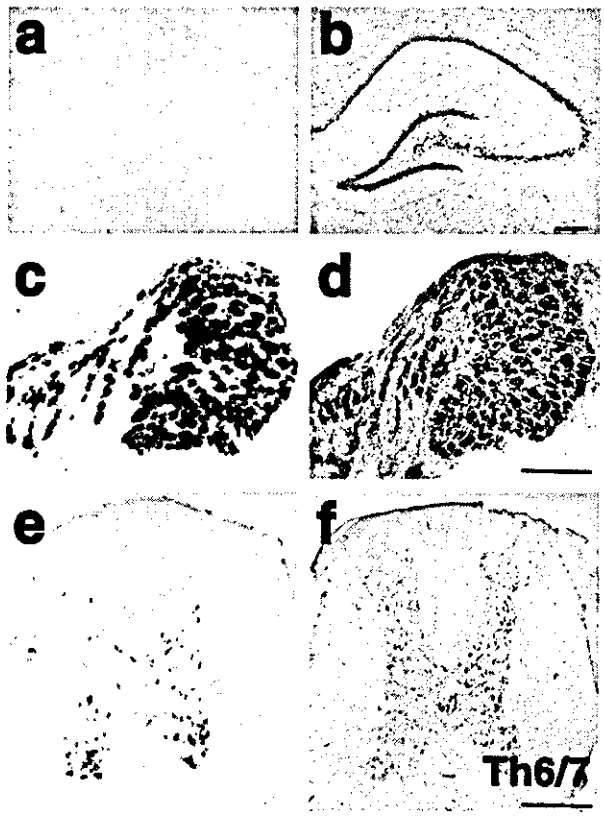

Fig. 6. Hybridization with antisense riboprobe (a, c, and e) and control Nissl staining (b, d, and f) of adult rat coronal sections. No significant staining was observed in hippocampal formation (a, b). Neurons in dorsal root ganglia were intensely stained with galectin-1 (c, d). Ventral motor neurons were positively stained in the spinal cord (thoracic: th6/7). Scale bar=0.2 mm.

level of expression was not intense compared with the other brain regions. The results were identical with the previous report (Puche and Key, 1995).

Cerebral cortical areas

The expression of galectin-1 mRNA was essentially same throughout the neocortex and allocortex. The scattered staining pattern was detected in the layers IV–VI (data not shown), although the signal intensities were very weak. In the hippocampus formation, the expression of galectin-1 mRNA was barely detected (Fig. 6a).

Subcortical regions in the forebrain

Neuronal cell bodies of some regions were weakly labeled in the septum and amygdaloid complex including the endopiriform nuclei. In the preoptic and hypothalamic regions, neuronal cell bodies were weakly labeled with galectin-1 mRNA in paraventricular nucleus, arcuate nucleus and tuberomammillary nucleus. In the habenula, no labeled neuron was detected.

Lower brain stem

The signal intensities of galectin-1 positive neurons in the midbrain were stronger than those in the forebrain regions. Neuronal cell bodies of oculomotor nucleus (arrowheads in Figs. 3a and 3b) and magnocellular red nucleus (asterisks in Figs. 3a and 3b) showed prominent expression of galectin-1 mRNA. Neurons in dorsal raphe nucleus displayed weak expression of galectin-1 mRNA while neurons in trochlear nucleus (arrowheads in Fig. 3c and 3d) and mesencephalic reticular formation (asterisks in Fig. 3c and 3d) shows intense staining. As shown in Fig. 3e and 3f, neurons in pontine reticular formation and trigeminal motor nucleus expressed galectin-1 mRNA at high level. (Fig. 4a–f).

Spinal cord, dorsal root ganglia and autonomic ganglia

In the PNS, the galectin-1 mRNA was detected in the nucleus motorius lateralis at the level of cervical to sacral spinal cord. All the neurons of dorsal root ganglia expressed galectin-1 mRNA, while possible glial cells of small size did not seem to be labeled in this experimental condition. To further access the expression of galectin-1 in peripheral sensory neurons, trigeminal ganglia (TG) and nodose ganglia (NG) were analyzed by *in situ* hybridization analysis. The neurons of TG and NG did not show any signal of galectin-1 mRNA (data not shown). We also examined the autonomic ganglion neurons such as superior cervical ganglia and sphenopalatine ganglia and galectin-1 mRNA could not be detected (data not shown).

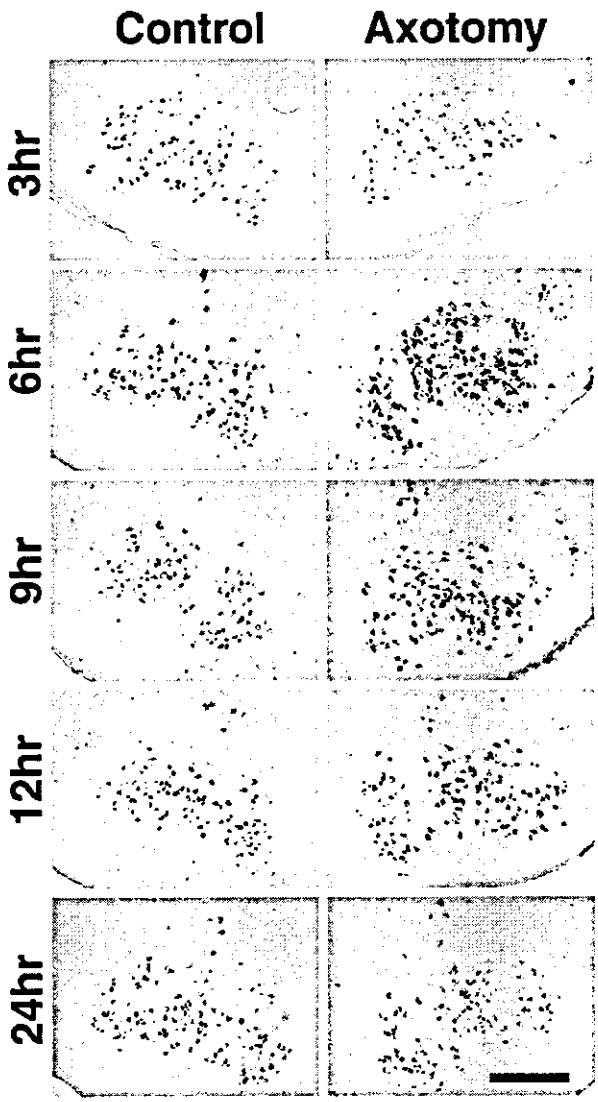

Fig. 7. Coronal sections containing bilateral facial nuclei were examined by *in situ* hybridization. The galectin-1 mRNA expression was transiently (6 h and 9 h after axotomy) upregulated in the motor neurons of the axotomized facial nucleus. No upregulation was detected in the control side. Scale bar=2 mm.

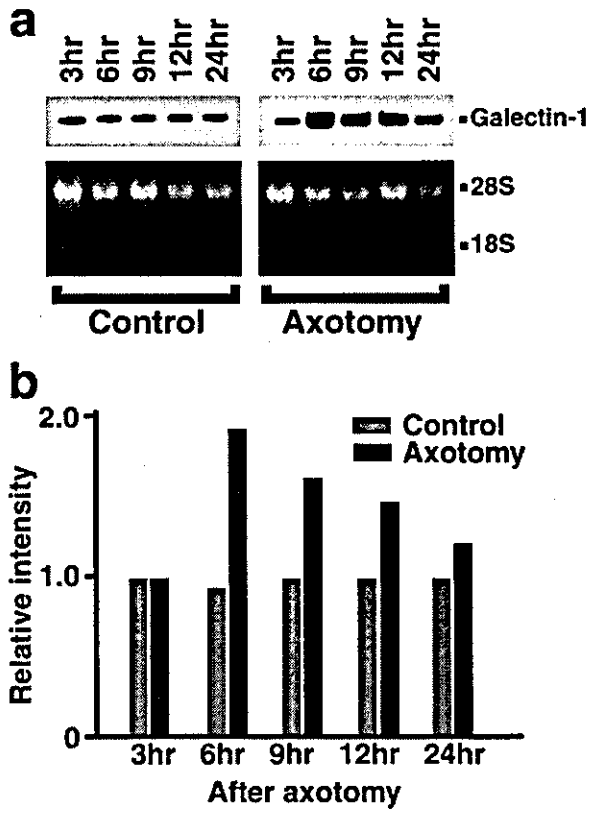

Fig. 8. Northern blot analyses were carried out to confirm the upregulation of galectin-1 mRNA (a). The bands corresponding to the 6 h to 9 h after axotomy significantly upregulated the galectin-1 mRNA compared with the non-operated control side (Top). The ethidium bromide staining of the gel indicated that the relatively equal amount of total RNA was loaded in this experiment (bottom). The radioactive intensity was measured using the image analyzer and plotted against time course after axotomy (b). Relative intensity per control (3 h) was shown. On the side of operation, the level of galectin-1 mRNA was increased by two-fold after 6–9 h after the facial nerve axotomy. Boxed: axotomy; Gray: control.

Non-neuronal cells

In addition to the neuronal expression, pinealocytes in the pineal gland expressed the high level of galectin-1 mRNA (Fig. 5e and 5f).

Axotomy of facial nerve and isciadic nerve

Following hemilateral axotomy of facial nerve at the surface of stylomastoideus foramen, the expression of galectin-1 mRNA in the facial nuclei was analyzed by the *in situ* hybridization analysis. Only on the side of the operation, facial neurons gave rise to a significant signal around 6 h and 9 h incubation after axotomy. No significant increase of galectin-1 mRNA was detected after 24 h incubation after axotomy (Fig. 7). To quantify the level of galectin mRNA, the Northern blot analysis was performed. The total RNA purified from the pooled facial nuclei from three independent experiments was analyzed at the indicated intervals after axotomy (3 h, 6 h, 9 h, 12 h, and 24 h). Expression of galectin-1 mRNA was upregulated from 6 h to 9 h interval after axotomy only on the side of the operation. By contrast, the opposite side of the facial nuclei did not show any increase of galectin-1 mRNA. The radioactive intensity was quantified using BAS5000 image analyzer and plotted against the time course after the axotomy. The level of galectin-1 mRNA was increased by two-fold compared with the non-operated control side (Fig. 8b). The ethidium bromide staining of the electrophoresed gel showed that the relatively equal amount of total RNA were loaded in this experiment (Fig. 8a, bottom).

DISCUSSION

Galectin-1 was described as a β-galactoside binding animal lectin, exhibiting its lectin activity only when it is reduced. Previously, it was reported that galectin-1 acts as a repair factor in peripheral nerve axotomy (Horie et

Table 1. Distribution of galectin-1 mRNA in the rat nervous system

Regions in the CNS examined[a]	Relative intensity on cell bodies[b]
Olfactory system	
Main olfactory bulb	
Mitral cells	1
Tufted cells	1
Granule cells	1
Scattered small cells	1
Accessory olfactory bulb	0
Anterior olfactory nucleus	0
Olfactory tubercle	
Pyramidal cells	0
Islands of Calleja	1
Neocortex	1
Limbic cortex	
Piriform cortex	1
Cingulate cortex	1
Retrosplenial cortex	1
Perirhinal cortex	0
Entorhinal cortex	0
Parasubicular cortex	0
Dentate gyrus	
Granule cells	0
CA4	0
Ammon's horn (CA1–CA3)	0
Septum	
Lateral septal nucleus	1
Medial septal nucleus	1
Septohypothalamic nucleus	0
Septofimbrial nucleus	1
Triangular septal nucleus	0
Nuclei of the diagonal band	0
Bed nucleus of the stria terminalis	1
Preoptic region	0
Amygdala	
Anterior amygdaloid area	1
Nucleus of the lateral olfactory tract	1
Cortical amygdaloid nucleus	1
Medial amygdaloid nucleus	0
Bed nucleus of the accessory olfactory tract	0
Posteromedial cortical amygdaloid nucleus	0
Lateral amygdaloid nucleus	1
Basolateral amygdaloid nucleus	
Ventral part	0
Other parts	0
Basomedial amygdaloid nucleus	1
Central amygdaloid nucleus	1
Dorsal endopiriform nucleus	1
Ventral endopiriform nucleus	1
Basal ganglia	
Caudate-putamen	0
Nucleus accumbens	1
Ventral pallidum	0
Globus pallidus	1
Entopenduncular nucleus	0
Subthalamic nucleus	0
Claustrum	0
Substantia nigra	1
Zona incerta	0
Hypothalamus	
Anterior hypothalamic area	0
Lateral hypothalamic area	0
Suprachiasmatic nucleus	0
Supraoptic nucleus	0
Paraventricular nucleus	1
Periventricular nucleus	0
Arcuate nucleus	1
Ventromedial hypothalamic nucleus	1
Dorsomedial hypothalamic nucleus	0
Tuberomammillary nucleus	1
Premammillary nucleus	0
Medial mammillary nucleus	0
Lateral mammillary nucleus	0
Habenula	
Medial habenular nucleus	0
Lateral habenular nucleus	0
Thalamus	
Thalamic reticular nucleus	1
Other nuclei	0
Lower brain stem	
Pretectum	
Anterior pretectal nucleus	1
Other nuclei	0
Red nucleus	3
Acueductal gray	0
Superior colliculus	0
Inferior colliculus	0
Nucleus of brachium of inferior colliculus	0
Mesencephalic reticular formation	
Ventral tegmental area	
Interpeduncular nucleus	
Parabrachial nuclei	
Oculomotor nucleus	3
Trochlear nucleus	3
Locus cereus	1
Laterodorsal tegmental nucleus	0
Barrington's nucleus	0
Nucleus O	0
Superior olivary nuclei	1
Nucleus of trapezoid body	0
Pontine reticular formation	3
Pontine tegmental reticular nucleus	2
Pontine nucleus	1
Abducens nuclei	3
Paragenual nucleus	0
Raphe nuclei	0
Medullary reticular formation	3
Trigeminary sensory complex	0
Trigeminal motor complex	3
Cochlear nuclei	
Dorsal nucleus	3
Ventral nucleus	3
Facial nucleus	3
Vestibular nuclei	0
Prepositus hypoglossal nucleus	3
Inferior olivary nuclei	1
Ambiguus nucleus	3
Nucleus of the solitary tract	1
External cuneate nucleus	0
Cuneate nucleus	0
Gracile nucleus	0
Cerebellum	

Table 1. continued

Regions in the CNS examined[a]	Relative intensity on cell bodies[b]
Deep nuclei	3
Cortex	
Purkinje cells	0
Granular cells	0
Golgi cells	0
Stellate cells	0
Spinal cord (C–S)	
Substantia gelatinosa	0
Ventral horn	2
Motor neurons	3
Central gray	0

[a] The brain regions were demarcated according to Paxinos and Watson (1986).
[b] Relative intensity on cell bodies: 3, very high; 2, high; 1, low; 0, background level.

al., 1999). Galectin-1 enhances axonal regeneration after nerve injury through promoting the reactive Schwann cells to migrate. But the expression analyses of galectin-1 in the nervous system were only limited in restricted areas. Thus we focused our attention on the topological analysis of galectin-1 mRNA in the brain. Immunohistochemistry using galectin-1 antibody cannot address the cell types that produce galectin-1, because galectin-1 was secreted from cells. Although the molecular mechanisms of galectin-1 secretion, even without signal leading peptide, were characterized in the case of muscle cells (Cooper and Barondes, 1990), the detailed molecular mechanisms remain to be solved. Thus *in situ* hybridization analysis is the only way to identify the galectin-1 producing cells. As previously reported, galectin-1 mRNA was detected at a high level in the discrete population of neurons of cerebral nuclei. Furthermore, galectin-1 was detected in cortical neurons at low level not only in the neurons, but also in the non-neuronal cells, such as pia mater, choroidal plexus, and pineal gland express galectin-1 mRNAs, although the physiological significance has not been elucidated.

Previously, galectin-1 null mutant mice were generated by homologous recombination in ES cells. Following transfer of this mutation into the germ line, the mice bearing null galecti-1 were analyzed (Poirier and Robertson, 1993). Surprisingly, the mice lacking the galectin-1 protein appear to develop normally. Adult mutant mice do not harbor any obvious phenotypic differences that distinguish them from wild-type siblings, although the further investigation using these null mutants will be required to reveal the physiological function of galectin-1 in the nervous system.

Recently, another protein family was found to share similar properties with galectin family in some respects, although they are not structurally related. Annexins, which had been previously considered as phospholipid-binding proteins, display a glycosaminoglycan-binding activity, and thus turned out to be new lectin molecules. Annexin II has been described as a regulatory factor that facilitates the expression of sensory neuron-specific tetrodotoxin-resistant sodium channel (Okuse et al., 2002). Annexin II light chain directly binds to the amino terminus of NaC1.8 and promotes the translocation of NaV1.8 to the plasma membrane to form a functional channel in response to tissue damage combined with growth factors such as NGF and TGF-α. Taken together the axonal growth activity of gaclectin-1, animal lectins may constitute a reactive pathway in the nervous system and play an important role in the nerve regeneration.

The expression of galectin-1 mRNA in the neurons of facial nuclei was transiently upregulated 6–9 h after facial nerve axotomy. This result suggests that the facial nerve injury can trigger the synthesis of galectin-1 in the neuronal cell bodies. The physiological role of this upregulation was not elucidated. In some cases, the upregulated galectin-1 may play a role in the inflammatory response after injury. The anti-inflammatory effect of galectin-1 was previously reported including the inhibition of chemical mediators of the inflammatory response (Rabinovich et al., 2000). It is also possible that upregulation of galectin-1, similar to neurotrophic factors and cytokines (Carlson et al., 1996; Lee et al., 1998), may help neuronal cells survive and regenerate neurites (Nishioka et al., 2002). Furthermore, upregulation of galectin-1 mRNA may increase galectin-1 in facial nerves resulting with increase of galectin-1 secretion. Some of secreted galectin-1 is briefly oxidized to become oxidized galectin-1 that loses lectin activity. Recent reports indicated that oxidized galectin-1 is essential *in vivo* for peripheral nerve regeneration after injury (Horie et al., 1999; Inagaki et al., 2000; Fukaya et al., 2002). Thus, oxidized galectin-1 could similarly work in facial motor neurons following facial nerve axotomy, although the precise mechanism how galectin-1 is secreted from neurons and other cells after axonal injury remains to be elucidated.

Acknowledgements—We thank Dr. Yoh Sasaki for technical assistance. We are indebted to Dr. Hitoshi Kawano, Tokyo Metropolitan Institute for Neuroscience, and Dr. Noboru Mizuno, National Institute for Physiological Science, for discussion and helpful comments. Grant Sponsor: Ministry of Health, Labor, and Welfare, Japan, Ministry of Education, Culture, Sports, Science and Technology, Japan, and the Sankyo Foundation of Life Science.

REFERENCES

Akazawa C, Shigemoto R, Bessho Y, Nakanishi S, Mizuno N (1994) Differential expression of five *N*-methyl-D-aspartate receptor subunit mRNAs in the cerebellum of developing and adult rats. J Comp Neurol 347:150–160.

Amano M, Calvan M, He J, Baum LG (2003) The ST6Gal I sialyltransferase selectively modifies *N*-glycans on CD45 to negatively regulate galectin-1-induced CD45 clustering, phosphatase modulation, and T cell death. J Biol Chem 278:7469–7475.

Barondes SH (1984) Soluble lectins: a new class of extracellular proteins. Science 223:1259–1264.

Barondes SH, Castronovo V, Cooper DW, Cummings RD, Drickamer K, Feizi T, Gitt MA, Hirabayashi J, Hughes C, Kasai K, Leffler H, Liu FT, Lotan R, Mercurio AM, Monsigny M, Pillai S, Poirier F, Raz A, Rigby PW, Rini JM, Wang JL (1994) Galectins: a family of animal β-galactoside-binding lectins. Cell 76:597–598.

Carlson CD, Bai Y, Ding M, Jonakait GM, Hart RP (1996) Interleukin-1 involvement in the induction of leukemia inhibitory factor mRNA

expression following axotomy of sympathetic ganglia. J Neuroimmunol 70:181–190.

Caron M, Bladier D, Joubert R (1990) Soluble galactoside-binding vertebrate lectins: a protein family with common properties. Int J Biochem 22:1379–1385.

Cooper DNW, Barondes SH (1990) Evidence for export of a muscle lectin from cytosol to extracellular matrix and for novel secretory mechanism. J Cell Biol 110:1681–1691.

Drickamer K (1988) Two distinct classes of carbohydrate-recognition domain in animal lectins. J Biol Chem 263:9557–9560.

Fukaya K, Hasegawa M, Mashitani T, Kadoya T, Horie H, Hayashi Y, Fujisawa H, Tachibana O, Kida S, Yamashita J (2003) Oxidized galectin-1 stimulates the migration of Schwann cells from both proximal and distal stumps of transected nerves and promotes axonal regeneration after peripheral nerve injury. J Neuropathol Exp Neurol 62:162–172.

Hirabayashi J, Kasai K (1993) The family of metazoan metal-independent β-galactoside-binding lectins; structure, function and molecular evolution. Glycobiology 3:297–304.

Horie H, Inagaki Y, Sohma Y, Nozawa R, Okawa K, Hasegawa M, Muramatsu N, Kawano H, Horie M, Koyama H, Sakai I, Takeshita K, Kowada Y, Takano M, Kadoya T (1999) Galectin-1 regulates initial axonal growth in peripheral nerves after axotomy. J Neurosci 19:9964–9974.

Hynes MA, Gitt M, Barondes SH, Jessell TM, Buck LB (1990) Selective expression of an endogenous lactose-binding lectin gene in subsets of central and peripheral neurons. J Neurosci 10:1004–1013.

Inagaki Y, Sohma Y, Horie H, Nozawa R, Kadoya T (2000) Oxidized galectin-1 promotes axonal regeneration in peripheral nerves but does not possess lectin properties. Eur J Biochem 267:2955–2964.

Lasky LA (1992) Selectins: interpreters of cell-specific carbohydrate information during inflammation. Science 258:964–969.

Lee SE, Shen H, Taglialatela G, Chung JM, Chung K (1998) Expression of nerve growth factor in the dorsal root ganglion after peripheral nerve injury. Brain Res 796:99–106.

Nishioka T, Sakumi K, Miura T, Tahara K, Horie H, Kadoya T, Nakabeppu Y (2002) FosB gene products trigger cell proliferation and morphological alteration with an increased expression of a novel processed form of galectin-1 in the rat 3Y1 embryo cell line. J Biochem (Tokyo) 131:653–661.

Okuse K, Malik-Hall M, Baker MD, Poon WYL, Kong H, Chao MV, Wood JN (2002) Annexin II light chain regulates sensory neuron-specific sodium channel expression. Nature 417:653–656.

Paxinos G, Watson C (1986) The rat brain in stereotaxic coordinates, 2nd edition. Sydney: Academic Press.

Poirier F, Robertson EJ (1993) Normal development of mice carrying a null mutation in the gene encoding the L14 S-type lectin. Development 119:1229–1236.

Puche AC, Key B (1995) Identification of cells expressing galectin-1, a galactose-binding receptor, in the rat olfactory system. J Comp Neurol 357:513–523.

Rabinovich GA, Sotomayor CE, Riera CM, Bianco I, Correa SG (2000) Evidence of a role for galectin-1 in acute inflammation. Eur J Immunol 30:1331–1339.

(Accepted 28 January 2004)

Human Molecular Genetics, 2003, Vol. 12, No. 16 **1945–1958**
DOI: 10.1093/hmg/ddg211

Ubiquitin carboxy-terminal hydrolase L1 binds to and stabilizes monoubiquitin in neuron

Hitoshi Osaka[1,2,†,‡], Yu-Lai Wang[1,†], Koji Takada[3], Shuichi Takizawa[1,4], Rieko Setsuie[1,5], Hang Li[1], Yae Sato[1,5], Kaori Nishikawa[1], Ying-Jie Sun[1], Mikako Sakurai[1,5], Takayuki Harada[1], Yoko Hara[1,6], Ichiro Kimura[6], Shigeru Chiba[4], Kazuhiko Namikawa[7], Hiroshi Kiyama[7], Mami Noda[5], Shunsuke Aoki[1] and Keiji Wada[1,*]

[1]Department of Degenerative Neurological Diseases, National Institute of Neuroscience, National Center of Neurology and Psychiatry, Kodaira, Tokyo, 187-8502, Japan, [2]Information and Cellular function, PRESTO, Japan Science and Technology Corporation (JST), Kawaguchi, Saitama 332-0012, Japan, [3]Department of Biochemistry 1, Jikei University School of Medicine, Minato-ku, Tokyo, 105-8461, Japan, [4]Department of Psychiatry and Neurology, Asahikawa Medical College, Asahikawa, 078-8510, Japan, [5]Laboratory of Pathophysiology, Graduate School of Pharmaceutical Sciences, Kyushu University, Higashi-ku, Fukuoka, 812-8582, Japan, [6]Department of Basic Human Science, School of Human Science, Waseda University, Tokorozawa, 359-1192, Japan and [7]Department of Anatomy and Neurobiology, Graduate School of Medicine, Osaka City University, Abeno-ku, Osaka, 545-8585, Japan

Received March 13, 2003; Revised June 6, 2003; Accepted June 17, 2003

Mammalian neuronal cells abundantly express a deubiquitylating enzyme, ubiquitin carboxy-terminal hydrolase 1 (UCH L1). Mutations in UCH L1 are linked to Parkinson's disease as well as gracile axonal dystrophy (*gad*) in mice. In contrast to the UCH L3 isozyme that is universally expressed in all tissues, UCH L1 is expressed exclusively in neurons and testis/ovary. We found that UCH L1 associates and colocalizes with monoubiquitin and elongates ubiquitin half-life. The *gad* mouse, in which the function of UCH L1 is lost, exhibited a reduced level of monoubiquitin in neurons. In contrast, overexpression of UCH L1 caused an increase in the level of ubiquitin in both cultured cells and mice. These data suggest that UCH L1, with avidity and affinity for ubiquitin, insures ubiquitin stability within neurons. This study is the first to show the function of UCH L1 *in vivo*.

INTRODUCTION

The small 76-amino acid protein ubiquitin (Ub) plays a critical role in many cellular processes, including the cell cycle, cell proliferation, development, apoptosis, signal transduction and membrane protein internalization (1). Moreover, Ub and/or Ub-containing protein aggregates are hallmarks of various neurodegenerative conditions (2). Fundamentally, monoubiquitylation constitutes a sorting signal for membrane proteins to the endosome–lysosomal pathway while polyubiquitylated proteins (covalently linked to Lys48 of Ub) are targeted to the 26S proteasome for degradation. At least three classes of enzymes are engaged in the ubiquitylation processes, namely the E1 (Ub-activating), E2 (Ub-conjugating) and E3 (Ub ligase) enzymes (1). Ubiquitylation also controls the sorting and localization of certain proteins in a reversible manner, much as phosphorylation modulates changes in the structure, activity and the localization of the target proteins. As such, deubiquitylating enzymes (DUBs) act analogously to phosphatases that function in phosphorylation processes (3).

DUBs are subdivided into Ub C-terminal hydrolases (UCHs) and Ub-specific proteases (UBPs). Both classes are thiol proteases that hydrolyze the isopeptide bond between the substrate and the C-terminal Gly76 of Ub. UCHs can hydrolyze bonds between Ub and small adducts or unfolded polypeptides *in vitro* (4). UCHs also can cleave Ub gene products very slowly

*To whom correspondence should be addressed at: Department of Degenerative Neurological Diseases, National Institute of Neuroscience, NCNP, Kodaira, Tokyo, 187-8502, Japan. Tel: +81 423461715; Fax: +81 423461745; Email: wada@ncnp.go.jp
†The authors wish it to be known that, in their opinion, the first two authors should be regarded as joint First Authors.
‡Present address:
Division of Neurology, Clinical Research Institute, Kanagawa Children's Medical Center, Yokohama, 232-8555, Japan.

in vitro, either tandemly conjugated Ub monomers (UbB, UbC) or Ub fused to small ribosomal proteins (L40, S27a), to yield free Ub or ribosomal proteins, respectively (4,5). Yeast expresses one UCH (YUH1) and 16 UBPs (Ubp1–16). Two YUH1 homologs, UCH L1 and UCH L3, have been characterized in mammals (6,7). UCH L1 and UCH L3 are both small proteins of ~220 amino acids that share more than 40% amino acid sequence identity. However, the distribution of these isozymes is quite distinct in that UCH L3 is expressed ubiquitously while UCH L1 is selectively expressed in neuronal cells and the testis/ovary (6,7).

UCH L1 is one of the most abundant proteins in the brain (1–5% of total soluble protein) and immunohistological experiments demonstrate that it is localized exclusively to neurons (6). Although the role of UCH L1 *in vivo* remains unclear, its abundance and specificity for neurons predict a role in neuronal cell function/dysfunction. Similar to Ub, UCH L1 is a constituent of cellular aggregates that are indicative of neurodegenerative disease such as Lewy bodies in Parkinson's disease (PD) (8). Indeed, an isoleucine-to-methionine substitution at amino acid 93 of UCH L1 was reported in a family with a dominant form of PD (9). We found that a *Uch l1* gene deletion in mice causes gracile axonal dystrophy (*gad*), a recessive neurodegenerative disease (10,11). These two examples of neurological disorders in both humans and mice prompted us to investigate the function of UCH L1 in neuronal cells.

We show here that the *gad* mouse is analogous to a *Uch l1* null mutant. Using this mouse and *Uch l1* transgenic mice, we report a novel *in vivo* role for UCH L1 in Ub homeostasis that was unexpected from previous *in vitro* work (12,13). Our data show that UCH L1 associates with Ub in neuronal cells and suggest that this association is important for the maintenance of mono-Ub levels in neurons. UCH L1 effectively upregulates Ub levels at the post-translational level, and this upregulation is probably based on the inhibition of Ub degradation by UCH L1.

RESULTS

UCH L1 is undetectable in the *gad* mouse

The *gad* mouse carries a deletion of a genomic fragment including exons 7 and 8 of *Uchl1* (10). Given such a substantial deletion, the protein encoded by the *gad* allele most likely lacks the core structure of UCH L1, thus predicating its instability [wild-type mouse UCH L1 was modeled using the crystal structure of human UCH L3 (14) as a template; see Fig. 1A]. Immunoblotting using polyclonal antibody to UCH L1 failed to detect UCH L1 in either soluble (10) or insoluble brain lysates from the *gad* mouse (data not shown). Thus, the *gad* mouse is analogous to a *Uch l1* null mutant. Next, we examined whether UCH L3, another UCH in the brain, is upregulated by this mutation. The *gad* mouse showed comparable levels of UCH L3 mRNA and protein (Fig. 1B). Therefore, the phenotype in the mouse does not appear to be modified by compensatory UCH L3 up-regulation. We then employed this mutant mouse to characterize UCH L1 substrates or associated proteins *in vivo*.

UCH L1 associates with Ub

There should be physiological substrates for UCH L1 that accumulate in the *gad* mouse. To facilitate isolation of such UCH L1 substrates or associated proteins, mutant UCH $L1^{C90S}$ was purified from an *E. coli* expression system. UCH $L1^{C90S}$ lacks Ub carboxy-terminal hydrolase activity but retains the ability to associate with Ub (4) (Table 1). As such, UCH $L1^{C90S}$ represented an ideal tool for the purpose of binding to and isolating *in vivo* protein substrates or associates for UCH L1. His-UCH $L1^{C90S}$ and Ni-Sepharose resin were employed in a pull-down assay using soluble brain lysates from wild-type and *gad* mice. Eluates from the resin were subjected to SDS–PAGE and SELDI (surface-enhanced laser desorption/ionization) time-of-flight (TOF) analysis. Relative to wild-type lysates, consistently elevated levels of proteins were not detected in the *gad* mice brains including putative substrates of poly-Ub. Rather, the level of an ~8 kDa protein was consistently lower in *gad* mice lysates (Fig. 1C; left panel; band intensity of *gad* to wild-type is 0.80 ± 0.09, $n = 3$). In both lysates, this protein band was immunoreactive with an antibody to Ub (Fig. 1C; right panel). In-gel digestion of this band followed by tandem liquid chromatography/mass spectrometry produced two peptide sequences—TLSYNIQKESTLHLVLR and TITLEVEPSDTIENVK—that were 100% identical to sequences within mouse Ub. In another pull-down assay, His-Ub pulled down a band corresponding to UCH L1 (Fig. 1D). SELDI analysis showed identical mass peak patterns for the Ub band from wild-type and *gad* mice (Fig. 1E) with a principal mass peak at 8560.8 *m/z*, consistent with the *m/z* expected for free mono-Ub (8564.8). Wild-type and *gad* mouse brain lysates were then subjected to gel filtration chromatography and immunoblotted with anti-UCH L1 or anti-Ub. In the fractions from the wild-type mouse, mono-Ub eluted over the range of ~10–50 kDa, overlapping significantly with the elution of UCH L1 (Fig. 1F). In fractions from the *gad* mouse, however, mono-Ub eluted exclusively at ~10–14 kDa. These data suggest that UCH L1 associates with mono-Ub.

Loss of UCH L1 decreases the level of Ub in neuron

The expression and localization of UCH L1 and mono-Ub in the mouse nerve system were examined. The nervous system is consisted of two types of cells, nerve cells (neurons) and glia (astrocytes, oligodendrocytes/schwann cells, microglia, ependymal cells). Immunofluorescence microscopy shows UCH L1 co-expresses with a neuron marker, neurofilament (NF), but not with an oligodendrocytes marker, proteolipid protein (PLP), and an astrocytes marker, glial fibrillary acidic protein (GFAP), thus supporting the neuron-specific expression of UCH L1 (6) (Fig. 2A). Then double immunofluorescence labeling was performed in neural tissue using UCH L1 antibody and polyclonal Ub antibody that predominantly recognizes free Ub (Sigma) (15). It was found that immunoreactivities to anti-UCH L1 and anti-Ub colocalized within the neuron (Fig. 2B, upper panel). Moreover, Ub immunoreactivity was reduced in neurons in *gad* mice (Fig. 2B, lower panel). In the peripheral nerve, neuronal axons are enwrapped by myelin of glial schwann cells that are immunoreactive to myelin basic protein antibody (Fig. 2C, right and left panels). Immunohistochemisty

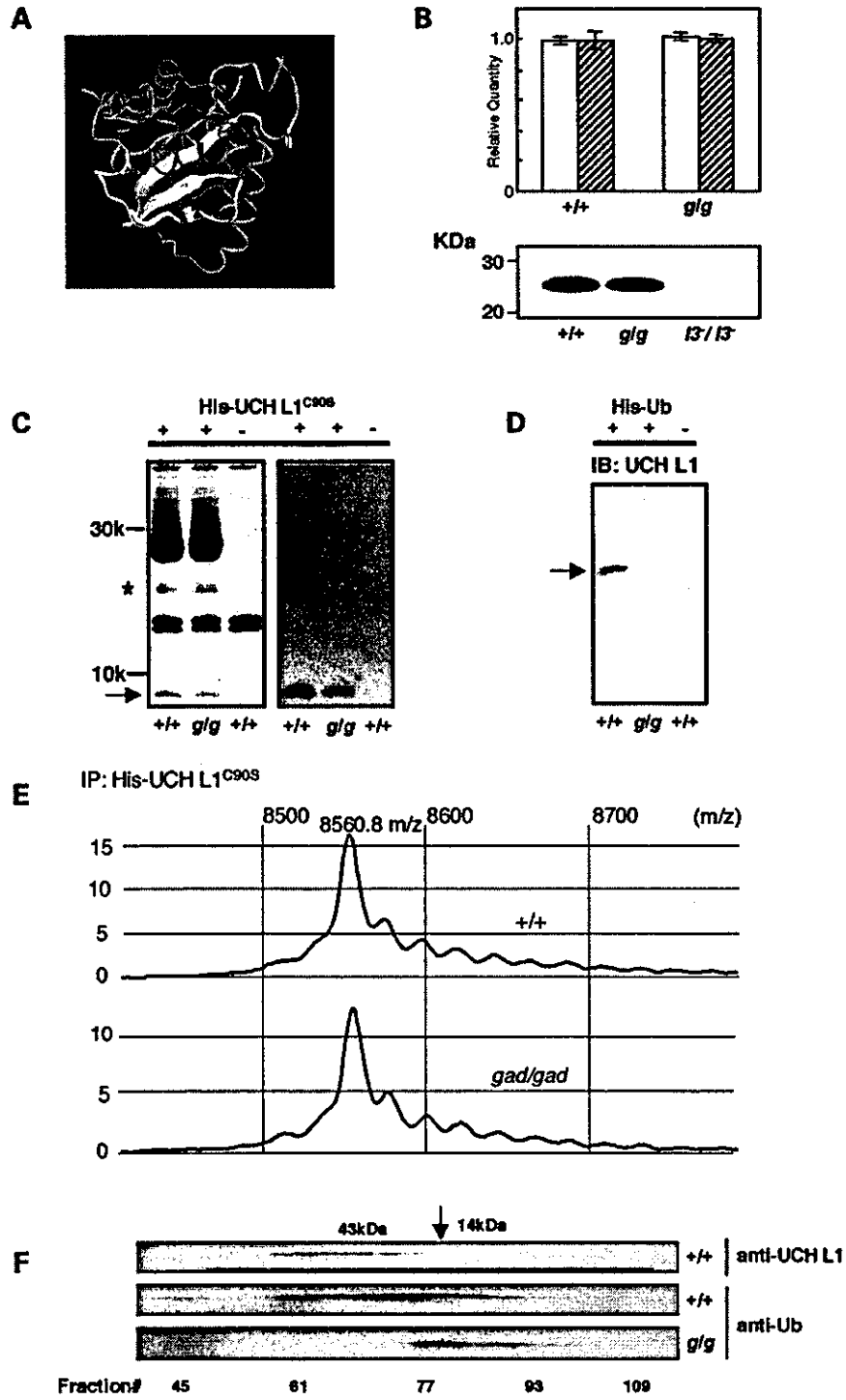

Figure 1. UCH L1 associates with ubiquitin. (**A**) Mouse UCH L1 was modeled after the crystal structure of human UCH L3 (14) using Insight II/Modeler (SGI). Secondary structures of the peptides deleted in the gracile axonal dystrophy (*gad*) mouse are shown in yellow. (**B**, upper panel) Quantitative RT–PCR for *Uch l3* was performed using total RNA from wild-type and *gad* (*gad/gad*) cerebra ($n = 3$ each). Mean values are shown with SEM. β-Actin (open bar) or GAPDH (solid bar) were used as internal controls. (B, lower panel) Soluble fractions (20 μg) of wild-type (+/+), the *gad* (g/g) and *Uch* $l3^{\Delta 3\text{-}7}$/*Uch* $l3^{\Delta 3\text{-}7}$($l3^{-}$/$l3^{-}$) (38) mouse brains were subjected to SDS–PAGE and immunoblotted with anti-UCH L1. (**C**) Eluates from pull-down assays using His-UCH $L1^{C90S}$ and brain lysate were subjected to SDS–PAGE, stained with Coomassie brilliant blue (left panel) and the band intensities to mono-Ub were compared. Eluates were also immunoblotted with monoclonal anti-Ub (right panel; Chemicon). Arrow shows the bands corresponding to mono-Ub. Asterisk shows the non-specific band that is co-purified during UCH L1 purification. (**D**) Eluates from pull-down assays using His-Ub and brain lysate were subjected to SDS–PAGE and immunoblotted with anti-UCH L1. The arrow shows the band corresponding to UCH L1. (**E**) Eluates from pull-down assays using His-UCH $L1^{C90S}$ and brain lysate were desalted with a C_{18} zip tip column and subjected to SELDI analysis. An *m/z* range near that expected for Ub ($m/z = 8562$) is presented. (**F**) Selected gel filtration chromatography fractions from wild-type brain lysates (upper and middle panels) and *gad* mice brain lysates (lower panel) were subjected to SDS–PAGE and immunoblotted with anti-UCH L1 (upper panel) or anti-Ub (middle and lower panels). The arrowhead and arrow correspond to the peak ovalbumin (43 kDa) and ribonuclease A (14 kDa) fractions, respectively.

Table 1. Kinetic parameters for hydrolysis of ubiquitin-7 amid-4 methyl-coumarin (Ub-AMC) by mouse UCH L1 and inhibition by Ub

Enzyme	K_m (μM)	k_{cat} (s^{-1})	$10^6 \times k_{cat}/K_m$ ($M^{-1}\,s^{-1}$)	K_i (μM)
UCH $L1^{WT}$	0.16	0.02	0.13	3.3
UCH $L1^{D30K}$	—	0	0	[0.28][b]
UCH $L1^{C90S}$	—	0[a]	0	[0.86][b]

Steady-state kinetic parameters were determined at 25°C in assay buffer. The mean values of three independent experiments are shown.
[a]No products were observed after 30 min with 5 mM enzyme.
Inhibitions were not assayed due to the lack of activity to substrates.
[b][Ratio of pulled down Ub to WT].

shows Ub immunoreactivity is decreased in neurons but not at glial schwann cells (Fig. 2D, middle panel).

Subsequently, cytosolic fractions of various nervous tissues that include both neuron and glia were subjected to SDS–PAGE and immunoblotted with a monoclonal Ub antibody that recognizes both free and conjugated Ub in denatured states (Chemicon) (15). The principal band corresponded to free mono-Ub, the intensity of which was reduced in *gad* mouse tissues (Fig. 3A, right panel) suggesting that mono-Ub is decreased in the absence of UCH L1 in the nervous system. A longer exposure or autoclaving the membrane enhanced the bands corresponding to Ub conjugates where no significant differences between wild-type and *gad* mice were observed (data not shown). Then mono-Ub levels in the nervous systems in <2-week-old wild-type and *gad* mice were measured by the radioimmunoassay (13). The inhibition rates for the ^{125}I-mono-Ub bound to antibody US-1 by brain lysates were compared with the standard curve generated by unlabeled mono-Ub (13). US-1 is specific antibody for free mono-Ub (13). Reduced levels of free mono-Ub (~20–30% reduction) were observed in each of the *gad* mouse tissues even at this early age (Fig. 3B; pathology in these mice was apparent only after >6 weeks). Immunoblotting and radioimmunoassay use cell lysates that contain both neuron and glia, which appears to be the reason for the apparent discrepancy between the large difference in Ub immuno-histochemistry in neurons and relatively smaller differences in mono-Ub levels in immunoblotting/radioimmunoassay.

These data show that Ub is associated with UCH L1 in neurons. Absence of UCH L1 reduces the mono-Ub level in neurons, which causes the reduction of overall mono-Ub level in the nervous system.

UCH L1 overexpression increases Ub levels

The effect of UCH L1 overexpression on Ub levels was examined in both cultured cells and transgenic mice. Adenovirus vectors expressing UCH L1 (adeno-*Uch l1*) or β-galactosidase (adeno-β-*gal*) were transfected into mouse embryonic fibroblasts (MEF) cells that do not express UCH L1. After transfection, UCH L1 was induced by Cre recombinase. Reactivitiy to anti-Ub exist at both nucleus and cytosol in adeno β-*gal* transfected and non-transfected MEF cells (Fig. 4B and C). Surprisingly, MEF cells transfected with adeno-*Uch l1* express UCH L1 dominantly at cytosol, where immunoreactivities to anti-Ub and anti-UCH L1

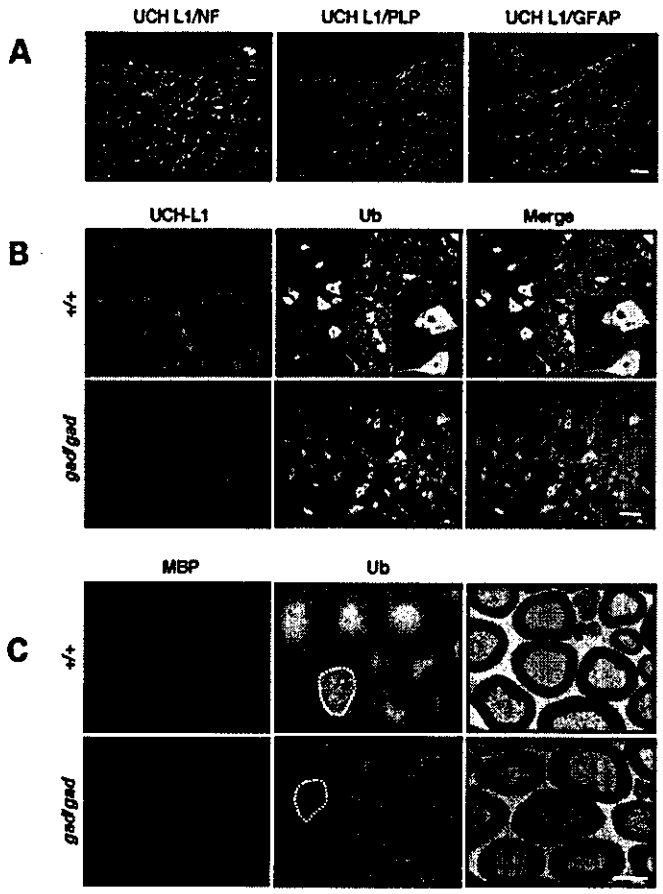

Figure 2. Loss of UCH L1 decreases ubiquitin immunoreactivity. Confocal laser scanning microscopy of mouse brain stem sections (**A, B**), sciatic nerve (**C**; left and middle panels) and electron microscopy for sciatic nerve (C; right panels) from 12-week-old wild-type or *gad* mice. (A) Immunohistochemistry to coronal sections at the brain stem, pons (fourth ventricule situates at the upper edges). Antibodies to a neuron marker, neurofilament (NF; left panel, green) and a glial oligodendrocytes marker, proteolipid protein (PLP; middle panel, green) and a glial astrocytes marker, glial fibrillary acidic protein (GFAP; right panel, green) were used for co-immunostaining with anti-UCH L1 (red). Immunoreactivity to anti-NF partially merges with that to anti-UCH L1. NFs exist at neuritis but not at a cell body of a neuron, whereas UCH L1 is expressed at both neuritis and cell bodies. Immunoreactivities to anti-PLP and anti-GFAP do not co-localize with that to anti-UCH L1. Scale bars, 40 μm. (B) Sections at neuronal nucleus in the pons from wild-type (upper panel) and *gad* mice (lower panel) were stained with anti-UCH L1 (green) and polyclonal anti-Ub (red; Sigma) on the same slide. Immunoreactivity to anti-UCH L1 is merged with that to anti-Ub. Moreover, immunoreactivity to anti-Ub is decreased in the *gad* mice that showed no reactivity to anti-UCH L1. Scale bars, 10 μm. Insets are images at four times higher magnification. (C) Sciatic nerve is composed of inner neuronal axon and outer myelin that is immunoreactive to anti-myelin basic protein (MBP, the marker of glial schwann cells, left panels). Immunoreactivity to anti-Ub in the neuronal axon (inside of dashed line) is decreased in the *gad* mouse, whereas the immunoreactivity to anti-Ub in glial myelin (outside the dashed line) is comparable between wild-type and *gad* mice. Electron microscopic images show fine structures of myelin and axon that are similar between wild-type and *gad* mouse in this 12 weeks of age (right panel). Scale bars, 10 μm.

are completely merged (Fig. 4A). Then the levels of Ub were compared by immnoblotting. The level of free mono-Ub as well as ubiquitylated proteins increased relative to the β-*gal* control at 24 h after UCH L1 induction (Fig. 4D; band intensity ratio of